[redacted]

[redacted]

# NASA TECHNICAL MEMORANDUM

NASA TM X-72763



NASA TM X-72763

## LOW-SPEED AERODYNAMIC CHARACTERISTICS OF A 9.3-PERCENT-THICK SUPERCRITICAL AIRFOIL SECTION

[redacted]

By Kevin W. Noonan and Robert J. McGhee



NATIONAL AERONAUTICS AND SPACE ADMINISTRATION
LANGLEY RESEARCH CENTER, HAMPTON, VIRGINIA 23665

[redacted]

[redacted]AL

| 1. Report No. | 2. Government Accession No. | 3. Recipient's Catalog No. |
|---|---|---|
| NASA TM X-72763 | | |

| 4. Title and Subtitle | 5. Report Date |
|---|---|
| Low-Speed Aerodynamic Characteristics of a 9.3-Percent-Thick Supercritical Airfoil Section | August 1975 |
| | 6. Performing Organization Code |

| 7. Author(s) | 8. Performing Organization Report No. |
|---|---|
| Kevin W. Noonan and Robert J. McGhee | |
| | 10. Work Unit No. |
| 9. Performing Organization Name and Address | 505-06-31-02 |
| NASA Langley Research Center<br>Hampton, VA 23665 | 11. Contract or Grant No. |
| | 13. Type of Report and Period Covered |
| 12. Sponsoring Agency Name and Address | Technical Memorandum |
| National Aeronautics & Space Administration<br>Washington, DC 20546 | 14. Sponsoring Agency Code |

15. Supplementary Notes

16. Abstract

An investigation has been conducted in the Langley low-turbulence pressure tunnel to determine the low-speed, two-dimensional characteristics of a 9.3-percent-thick supercritical airfoil. The airfoil was tested at Reynolds numbers (based on chord) from $2.9 \times 10^6$ to $16.8 \times 10^6$, at Mach numbers from 0.10 to 0.36, and at geometric angles of attack from -8° to 14°.

| 17. Key Words (Suggested by Author(s)) | 18. Distribution Statement |
|---|---|
| Aerodynamics<br>Supercritical Airfoil | [redacted] |

| 19. Security Classif. (of this report) | 20. Security Classif. (of this page) | 21. No. of Pages | 22. Price |
|---|---|---|---|
| [redacted] | Unclassified | 49 | STIF |

[redacted]

[redacted] CONFIDENTIAL [redacted] CLASSIFIED
[redacted] TO GENERAL DECLASSIFICATION SCHEDULE OF
EXECUTIVE ORDER [redacted] AUTOMATICALLY DOWNGRADED
AT TWO YEAR [redacted] INTERVALS AND DECLASSIFIED ON DEC 31
1981.

[redacted]

[redacted]

# LOW-SPEED AERODYNAMIC CHARACTERISTICS OF A 9.3-PERCENT-THICK SUPERCRITICAL AIRFOIL SECTION

By Kevin W. Noonan and Robert J. McGhee

Langley Research Center

## SUMMARY

An investigation has been conducted in the Langley low-turbulence pressure tunnel to determine the low-speed, two-dimensional characteristics of a 9.3-percent-thick supercritical airfoil. The airfoil was tested at Reynolds numbers (based on chord) from $2.9 \times 10^6$ to $16.8 \times 10^6$, at Mach numbers from 0.10 to 0.36, and at geometric angles of attack from -8° to 14°.

The results of this investigation indicate that at a Mach number of 0.20 the maximum lift coefficients varied from 1.66 to 1.80 for the range of test Reynolds numbers and that they were reduced by about 0.4 with the application of NACA standard roughness. The maximum lift coefficients at all test Reynolds numbers were limited by the separation of the tunnel sidewall boundary layer prior to the separation of the flow in the center span of the model. For the range of test Mach numbers at a constant Reynolds number of $4.0 \times 10^6$, the maximum lift coefficients varied from 1.92 to 1.16. The minimum drag coefficient was unchanged for the range of Reynolds numbers and Mach numbers of this investigation.

## INTRODUCTION

Supercritical airfoils have been developed primarily to extend the cruise Mach number beyond that of conventional airfoils (refs. 1, 2, & 3). These new types of airfoils operate efficiently at supercritical Mach numbers by minimizing the energy losses due to shock waves and the design approach to achieve this objective is explained in references 1 and 2. As part of the overall

[redacted]

investigation of these types of airfoils, the present investigation was conducted to determine the effect of changes in Reynolds number on the low-subsonic aerodynamic characteristics of a 9.3-percent-thick supercritical airfoil. The low-speed aerodynamic characteristics of this airfoil would be expected to be representative of other supercritical airfoils of about the same thickness ratio. The data obtained in the present investigation at a Reynolds number of $2.9 \times 10^6$ have been compared with data on a similar model tested in the tunnel of reference 4 and the low-turbulence pressure tunnel. The results have also been compared with calculations using a low-speed viscous flow theory.

The investigation was conducted in the Langley low-turbulence pressure tunnel at Reynolds numbers (based on chord) from $2.9 \times 10^6$ to $16.8 \times 10^6$, at Mach numbers from 0.10 to 0.36, and at geometric angles of attack from -8° to 14°. The airfoil with NACA standard roughness applied was also tested at three Reynolds numbers.

## SYMBOLS

The units used for the physical quantities of this paper are given both in the International System of Units (SI) and in the U.S. Customary Units. The measurements and calculations were made in the U.S. Customary Units.

$c$ airfoil chord, 0.6 m (23.622 in.)

$c_c$ section chord-force coefficient, $\int C_p \, d\left(\frac{z}{c}\right)$

$c_d$ section drag coefficient, $\frac{2}{c}\int \left(\frac{p_1}{p_\infty}\right)^{1/2\gamma} \left(\frac{q_1}{q_\infty}\right)^{1/2} \left[\left(\frac{p_2}{p_\infty}\right)^{1/2} - \left(\frac{q_2}{q_\infty}\right)^{1/2}\right] dh$

$c_l$ section lift coefficient, $c_n \cos \alpha - c_c \sin \alpha$

$c_{m,le}$ section pitching-moment coefficient about airfoil leading edge, $\int C_p \, d\left(\frac{z}{c}\right) \frac{z}{c} - C_p \, d\left(\frac{x}{c}\right) \frac{x}{c}$

$c_m$ section pitching-moment coefficient about the quarter chord point,

$$c_m = c_{m,le} + c_n\,(0.25)$$

$c_n$ section normal-force coefficient, $\int C_p\, d\left(\frac{x}{c}\right)$

$C_p$ static pressure coefficient, $\frac{p_l - p_\infty}{q_\infty}$

M Mach number

p static pressure, $n/m^2$ (psi)

q dynamic pressure, $1/2\ \rho v^2\ N/m^2$ (psi)

R Reynolds number based on airfoil chord

t airfoil thickness, cm (in.)

v velocity, m/sec (ft/sec)

x airfoil abscissa, cm (in.)

y distance from center span of airfoil measured along the airfoil span, cm (in.)

z airfoil ordinate, cm (in.)

$z_c$ ordinate of airfoil camber line, cm (in.)

$\alpha$ angle of attack, angle between airfoil chord line and airstream direction, deg

$\rho$ density, $Kg/m^3$ ($slugs/ft^3$)

Subscripts:

l local

$\infty$ free stream

1 tunnel station at the plane of the wake rake

2 tunnel station downstream of model where static pressure is equal to free stream static, $p_\infty$

Superscripts:

' quantities have been corrected for wall interference effects

Abbreviations:

BRWT Boeing Research Wind Tunnel

LTPT low turbulence pressure tunnel

## APPARATUS AND METHODS

### Model

The airfoil profile, thickness distribution and camber line are presented in figure 1 and the coordinates are presented in table I. The airfoil model was machined from an aluminum billet and had a chord of 0.6 m (23.622 in.) and a span of 1.002 m (1.670c) which permitted the model to extend through sealing end plates at the tunnel wall for attachment purposes (fig. 2). Pressure tubes were installed in channels cut into the model and were secured in place by a plastic resin; the final airfoil contour was finished to a polished surface. The model was equipped with 59 pressure orifices (30 upper surface and 29 lower surface) on the center span and 36 pressure orifices across the span of the upper surface. The locations of all the pressure orifices are presented in table II. The 0.813 mm (0.032 in.) diameter orifices were drilled perpendicular to the local surface contour.

A second model of the 9.3-percent-thick supercritical airfoil was also tested in LTPT. This model was fabricated for the investigation described in reference 4 and details of the construction of that model are given in volume II of that reference. The measured coordinates of this second model agreed with the measured coordinates of the present model within fabrication tolerances.

[redacted]

Wind Tunnel

The Langley low-turbulence pressure tunnel is a closed-throat single-return tunnel which is generally operated at stagnation pressures from 1 to 10 atmospheres. (See ref. 5). The tunnel-empty Reynolds number and Mach number attainable at one atmosphere are $8.86 \times 10^6$ per meter and 0.42 respectively and the corresponding values attainable at 10 atmospheres are $49.0 \times 10^6$ per meter and 0.22. The test section is 0.9144 m (3 ft) wide by 2.286 m (7.5 ft) high.

The airfoil was attached to 1.016 m (3.33 ft) diameter end plates which were rotated by an hydraulic acuator to position the airfoil at the desired angle of attack. The model spanned the width of the tunnel with the quarter chord point coincident with the rotational axis of the end plates. The installation of the model in the wind tunnel is shown in figure 2 and a typical photograph of a model mounted in the tunnel is presented in figure 3.

APPARTUS

Wake Rake.- A wake rake was located 1.03 chords downstream of the airfoil trailing edge and on the tunnel center line to measure profile drag. This rake was held in position by two horizontal support arms which were rigidly attached to one tunnel sidewall as shown in the photograph, figure 3. The rake had 31 total pressure tubes and 5 static pressure tubes. As indicated in figure 4, the spacing between adjacent total pressure tubes was increased from 0.318 cm (0.0052c) to 0.635 cm (0.011c) and then to 1.27 cm (0.021c) with increasing distance of the tubes from the rake center line; the spacing between adjacent static pressure tubes was 11.45 cm (0.19c). Both the total pressure and the static pressure tubes consist of 1.524 mm (0.060 in.) diameter steel tubing. The ends of the total pressure tubes were flattened to 1.016 mm (0.040 in.) fo

[redacted]

[redacted]

a distance of 6.35 mm (0.25 in.) to minimize the effects of pressure gradients across the tube opening.

Instrumentation.- All measurements made during the test program were obtained with the use of a high-speed, computer-controlled data acquisition system and were recorded by a high-speed tape recording unit. Each of the two basic tunnel pressures from which all the free-stream conditions were determined were measured by precision quartz pressure sensors. The stagnation temperature was measured with a thermocouple and the angle of attack was determined from the output of a digital shaft encoder attached to a pinion engaging a rack on the supporting end plates. The airfoil surface pressures and wake pressures were measured with automatic pressure-ranging transducers connected to the model orifices and wake rake by means of an automatic pressure scanning system.

## Tests and Methods

The tests were conducted at Reynolds numbers from $2.9 \times 10^6$ to $16.8 \times 10^6$, at Mach numbers from 0.10 to 0.36, and at geometric angles of attack from -8° to 14°. Flow visualization studies were made at Reynolds numbers of $2.9 \times 10^6$ and $8.8 \times 10^6$ with tufts attached to the upper surface of the airfoil. The effects of NACA standard roughness, which consisted of #60 Carborundum grit applied from the leading edge over a surface length of 0.08c on both surfaces (ref. 6), were determined at three Reynolds numbers. In addition, a strip of Carborundum grit 2.54 mm (0.10 in.) wide with a coverage density of 5 to 10 percent was placed at several different chord locations at a Reynolds number of $5.9 \times 10^6$. The grit size was determined by the method of reference 7.

Section normal-force and pitching-moment coefficients were calculated from the surface pressures by a trapezoidal integration of the pressure coefficients. The section drag coefficients were calculated from the wake pressures

[redacted]

[redacted]

by trapezoidal integrations of the point drag coefficients as described in reference 8. The wake static pressures used in the drag calculation were obtained from tunnel sidewall orifices located at the same longitudinal tunnel stations as the tips of the rake total pressure tubes. As noted in reference 9, the wake static pressure measurements made with the wake rake static pressure tubes were influenced by the rake body and therefore were not used.

The wind tunnel boundary corrections computed by the method of reference 10 for a representative case ($\alpha = 10°$) were 2 percent or less and for this reason they have not been applied except in one case. The corrections were applied to the LTPT data in the comparison of the LTPT data with the data of reference 4. (See fig. 11.).

## PRESENTATION OF RESULTS

The results of this investigation are presented in the following figures:



[redacted]

[redacted]



## DISCUSSION

### Two-Dimensionality of Flow

Spanwise airfoil surface pressures at three nominal chordwise locations were measured for all test conditions to evaluate the two-dimensionality of the flow and the representative pressure distributions for the lowest, an intermediate, and the highest test Reynolds number are presented in figure 5. Examination of all the spanwise pressure distributions at a Mach number of 0.20 clearly indicated the two-dimensionality of the flow to at least an angle of attack of 12.0°. Some asymmetry in the pressure distributions was indicated at angles of attack above 12.0° and prior to the stall angles of attack at all but the lower two test Reynolds numbers; this flow breakdown was very near $(c_l)_{max}$ in all cases. Tuft studies were made at two Reynolds numbers to visualize the development of the non-two-dimensional flow field. Tuft photographs for $R = 8.8 \times 10^6$ are presented in figure 6.



[redacted]

For $2.9 \times 10^6$ (fig. 5(a)) Reynolds number, a loss of two-dimensionality is not clearly indicated by the spanwise pressure distributions until the airfoil has reached the stall angle of attack, 13.0°. Tuft studies made at this Reynolds number did show that a large region of separated flow existed near one tunnel sidewall at the angle of attack for $(c_l)_{max}$, 12.8°. The addition of the tufts probably disturbed the flow enough to cause the wall boundary-layer separation but this suggests that the stall was precipitated by a separation of the wall boundary layer. Figures 5(b) and 5(c) clearly indicate a loss of two-dimensional flow occurring at 13.3° and 12.1° respectively for Reynolds numbers of $8.8 \times 10^6$ and $16.8 \times 10^6$. Tuft photographs (fig. 6) illustrate the development of a region of separated flow near the tunnel sidewall at $R = 8.8 \times 10^6$.

The loss of two-dimensional flow observed during this investigation is believed to be due to a nonsymmetric separation of the tunnel sidewall boundary layers in the presence of the large adverse pressure gradient near the airfoil leading edge. Separation of the tunnel sidewall boundary layers prior to the separation of the flow in the center span of the airfoil has been observed previously in LTPT (ref. 11).

## Chordwise Pressure Distributions

The chordwise pressure distributions for the lowest, an intermediate, and the highest test Reynolds number are presented in figures 7(a) - 7(c). The pressure distributions for all test Reynolds numbers at a Mach number of 0.20 have a sharp minimum pressure peak at approximately 0.006 on the upper surface for angles of attack of 4° and higher, and a region of increasing pressures on the lower surface beginning at 0.65c and extending to 0.95c at all test angles of attack. The flat upper surface pressure distribution usually associated with supercritical airfoils is present for angles of attack from -4° to 0°.

At the lowest test Reynolds number of $2.9 \times 10^6$, the pressure distribution at an angle of attack of 13.0° indicates a complete collapse of the upper surface flow which is characteristic of a leading-edge type of stall. At the intermediate and the highest test Reynolds numbers, the pressure distributions indicate an unsteady pressure recovery on the upper surface at angles of attack of 13.3° and 12.0° and higher, respectively. These high angle of attack pressure distributions are influenced by the separated tunnel wall boundary layer and cannot be representative of two-dimensional flow.

## Lift

The lift curve slope of the 9.3-percent-thick supercritical airfoil is about 0.11 per degree for the range of Reynolds numbers and Mach numbers of this investigation (fig. 8). The slope is also unchanged by the addition of either NACA standard roughness at three test Reynolds numbers or by a strip of roughness (at several chordwise locations) at $5.9 \times 10^6$ (fig. 14(a)). For a Reynolds number of $2.9 \times 10^6$ (fig. 11), the slope on the present model is slightly higher than that measured on a similar model tested in another low-speed wind tunnel (ref. 4). However, the slopes measured on the present model are identical with those measured on the model of reference 4 during a test of that model in the low-turbulence pressure tunnel at Reynolds numbers from $2.9 \times 10^6$ to $11.6 \times 10^6$ (fig. 12(a)).

The maximum lift coefficient increases from 1.66 to 1.80 for an increase in Reynolds number from $2.9 \times 10^6$ to $4.0 \times 10^6$ and then decreases gradually to 1.66 with further increases in Reynolds number to $16.8 \times 10^6$ (fig. 8(a)). The maximum lift coefficients at all test Reynolds numbers were limited by a separation of the tunnel sidewall boundary layer prior to the separation of the flow in the center span of the airfoil. At $2.9 \times 10^6$, the decrease in maximum lift

coefficient due to a loss of two-dimensional flow was determined to be 0.06 by a comparison of the LTPT data obtained on the model of reference 4 with the data from the reference 4 facility, which employs a wall boundary-layer control system (fig. 11). The maximum lift coefficients obtained in the present investigation are 0.09 to 0.11 higher than those obtained in the LTPT test of the reference 4 model at Reynolds numbers of $5.9 \times 10^6$ and higher (fig. 12(a)). The reason for the close agreement at only the lowest test Reynolds number is not known.

The application of NACA standard roughness reduced the maximum lift coefficients by 0.35 to 0.43 from the smooth surface case at all three test Reynolds numbers (fig. 8(a)) and the maximum lift coefficients were less sensitive to the increases in Reynolds numbers. The effects of the addition of a narrow roughness strip at three different chordwise stations were investigated on the model of reference 4 at a Reynolds number of $5.9 \times 10^6$ (fig. 14). The maximum lift coefficients were essentially unchanged by the addition of the roughness strip at all three locations.

Some low-speed Mach number effects are shown in figure 8(b) for a Reynolds number of $4.0 \times 10^6$. The maximum lift coefficients decrease from 1.92 to 1.16 with increases in Mach number from 0.10 to 0.36. At Mach numbers as high as 0.20, the airfoil pressure distributions indicate no supercritical flow on the airfoil surface. An increase in Mach number from 0.10 to 0.15 results in a large decrease in maximum lift coefficient but a further increase to 0.20 results in a small increase in maximum lift coefficient. This effect may be related to the stability of a separation bubble which is generally present on airfoils that stall from the leading edge. At Mach numbers higher than 0.20, the decrease in maximum lift coefficient with increasing Mach number is believed

to be due to the onset of supercritical flow near the leading edge at progressively lower angles of attack.

The maximum lift coefficients of the NASA supercritical airfoil compare favorably with those of several NACA airfoils which have nearly the same thickness ratio and camber and were tested in the same facility (fig. 15). The maximum lift coefficients of the supercritical airfoil are equal to or exceed those of the three conventional airfoils at Reynolds numbers up to $6.0 \times 10^6$ and at $9.0 \times 10^6$ its value is exceeded only by that of the NACA 23012 airfoil.

In figure 16, the lift curves at the lowest and the highest test Reynolds numbers are compared with a low-speed viscous flow theory of reference 12 and with a recent modification of the reference 12 theory (ref. 13). The modification to the theory is primarily a change in the procedure for calculation of the drag coefficient. For a Reynolds number of $2.9 \times 10^6$ (fig. 16(a)), the lift-curve slopes predicted by both the theory and the modified theory are essentially the same as the experimental slope. At $16.8 \times 10^6$, the slope predicted by the theory is also the same as the experimental but the slope is underpredicted by the modified theory. The maximum lift coefficients at both Reynolds numbers are greatly overpredicted by the theory and the modified theory. The close agreement of the experimental and analytical lift curves up to $(c_l)_{max}$ is typical only for airfoils that have no separation up to that condition i.e., for airfoils that stall from the leading edge.

## Pitching-Moment Characteristics

The quarter chord pitching-moment coefficients show essentially no change with increases in Reynolds number from $2.9 \times 10^6$ to $16.8 \times 10^6$ (fig. 9(a)) or with increases in Mach number from 0.10 to 0.36 (fig. 9(b)). The addition of NACA standard roughness reduces the coefficients by a small amount from the

[redacted]

smooth surface case at all three test Reynolds numbers but does not change the insensitivity to Reynolds number. The pitching-moment coefficients measured on the model of reference 4 in LTPT are less negative than those measured on the same model in the reference 4 facility by about 0.01 (fig. 11) and those measured in the present investigation by about 0.015 (fig. 12(b)). In figure 13, the pressure distributions measured on the model of reference 4 in LTPT and those measured in the present investigation at nearly the same angle of attack show small differences, but over a large percentage of the chord. These differences result in a 0.015 difference in pitching-moment coefficients. The pitching-moment coefficients predicted by theoretical methods agree very well with the experimental data as shown in figure 16.

Drag

The minimum drag coefficient with a smooth model surface is 0.0085 for all test Reynolds numbers and the usual decrease in drag coefficients with increasing Reynolds number is significant only at lift coefficients above about 0.80 (fig. 10(a)). With NACA standard roughness applied, the entire drag curve is lowered with increases in Reynolds number and the minimum drag level is 0.0010 to 0.0025 higher than the corresponding model smooth case. The minimum drag coefficient is unchanged by increases in Mach number from 0.10 to 0.36 as shown in figure 10(b). At Mach numbers higher than 0.20, the abrupt increase in the slope of the drag curve occurs at lower lift coefficients with increases in Mach number and this is attributed to a small region of supersonic flow developing near the airfoil leading edge at lower angles of attack. The drag coefficients measured on the model of reference 4 in LTPT agree well with the data from the reference 4 facility and data from the present investigation at lift coefficients up to 0.8 (fig. 11); a good agreement of the drag coefficients

[redacted]

[redacted]

measured on two models extends to higher lift coefficients with increasing Reynolds number (fig. 12(c) & (d)). The drag level of the reference 4 model increased by about 0.0010 with the application of a narrow strip of roughness at the 0.05c location but only by about 0.0005 with applications at 0.10c and 0.20c. (See fig. 14(c).) The drag coefficients predicted by both analytical methods are substantially different from the experimental values at the lowest and the highest test Reynolds number as shown in figure 16.

## CONCLUSIONS

An investigation has been conducted in the Langley low-turbulence pressure tunnel to determine the low-speed, two-dimensional characteristics of a 9.3-percent-thick supercritical airfoil. The airfoil was tested at Reynolds numbers from $2.9 \times 10^6$ to $16.8 \times 10^6$, at Mach numbers from 0.10 to 0.36, and at geometric angles of attack from -8° to 14°.

The results presented indicate that at a Mach number of 0.20 the maximum lift coefficients increased from 1.66 to 1.80 for an increase in Reynolds number from $2.9 \times 10^6$ to $4.0 \times 10^6$ and then decreased gradually to 1.66 with f - ther increases in Reynolds number to $16.8 \times 10^6$. The maximum lift coefficients at all test Reynolds numbers were limited by a separation of the tunnel sidewall boundary layer prior to the separation of the flow in the center span of the model. At the lowest test Reynolds number, the incremental decrease in maximum lift coefficient was determined to be 0.06 by comparison of the low-turbulence pressure tunnel data with data from another low-speed wind tunnel employing sidewall boundary-layer control. The application of NACA standard roughness reduced the maximum lift coefficients by about 0.40 but the application of roughness strips did not change the $(c_l)_{max}$ values at $5.9 \times 10^6$. For a Reynolds number of $4.0 \times 10^6$, the maximum lift coefficients decreased from



[redacted]

[redacted]

1.92 to 1.16 for an increase in Mach number from 0.10 to 0.36. Although the maximum lift coefficients were limited by facility problems, the values compare favorably with those of conventional low-speed airfoils of similar thickness and camber that were tested in the low-turbulence pressure tunnel. The minimum drag coefficient was 0.0085 for the range of Reynolds numbers and Mach numbers of this investigation.

## REFERENCES


1. Whitcomb, Richard T.; and Clark, Larry R.: An Airfoil Shape for Efficient Flight at Supercritical Mach Numbers. NASA TM X-1109, 1965.
2. Harris, Charles D.: Wind-Tunnel Investigation of Effects of Trailing-Edge Geometry on a NASA Supercritical Airfoil Section. NASA TM X-2336, 1971.
3. McGhee, Robert J.; and Bingham, Gene J.: Low-Speed Aerodynamic Characteristics of a 17-Percent-Thick Supercritical Airfoil Section, Including a Comparison Between Wind-Tunnel and Flight Data. NASA TM X-2571, 1972.
4. Omar, E.; Zierten, T.; and Mahal, A.: Two-Dimensional Wind-Tunnel Tests of a NASA Supercritical Airfoil With Various High Lift Systems, Vol. I. NASA CR-2214, 1972.
5. von Doenhoff, Albert E.; and Abbott, Frank T., Jr.: The Langley Two-Dimensional Low-Turbulence Pressure Tunnel. NACA TN-1283, 1947.
6. Abbott, Ira H.; von Doenhoff, Albert E.; and Stivers, Louis S., Jr.: Summary of Airfoil Data. Report 824, 1945.
7. Braslow, Albert L.; and Knox, Eugene C.: Simplified Method for Determination of Critical Height of Distributed Roughness Particles for Boundary-Layer Transition at Mach Numbers From 0 to 5. NACA TN-4363, 1958.


[redacted]

8. Baals, Donald D.; and Mourhess, Mary J.: Numerical Evaluation of the Wake Survey Equations for Subsonic Flow Including the Effects of Energy Addition. NACA WRL-5, 1945.

9. McGhee, Robert J.; and Beasley, William D.: Low-Speed Aerodynamic Characteristics of a 17-Percent-Thick Airfoil Section Designed For General Aviation Applications. NASA TN D-7428, 1973.

10. Allen, H. Julian; and Vincenti, Walter G.: The Wall Interference in a Two-Dimensional Flow Wind Tunnel With Consideration of the Effects of Compressibility. NACA Report 782, 1944.

11. Bingham, Gene J.; and Chen, Allen Wen-shin: Low-Speed Aerodynamic Characteristics of an Airfoil Optimized for Maximum Lift Coefficient. NASA TN D-7071, 1972.

12. Stevens, W. A.; Goradia, S. H.; and Braden, J. A.: Mathematical Model for Two-Dimensional Multi-Component Airfoils In Viscous Flow. NASA CR-1843, 1971.

13. Smetana, F. O.; Summey, D. C.; Smith, N. S.; and Carden, R. K.: Light Aircraft Lift, Drag, And Moment Prediction - A Review And Analysis. NASA CR-2523, 1975.

TABLE I.- COORDINATES FOR THE 9.3-PERCENT-THICK

SUPERCRITICAL AIRFOIL

[Stations and ordinates given in percent airfoil chord]

| Stations | Upper surface | Stations | Lower surface |
|---|---|---|---|
| 0.00 | 0.00 | 0.00 | 0.00 |
| .10 | .62 | .10 | - .62 |
| .20 | .86 | .20 | - .86 |
| .30 | 1.04 | .30 | - 1.04 |
| .40 | 1.19 | .40 | - 1.19 |
| .60 | 1.41 | .60 | - 1.41 |
| .80 | 1.58 | .80 | - 1.58 |
| 1.00 | 1.72 | 1.00 | - 1.72 |
| 1.25 | 1.87 | 1.25 | - 1.87 |
| 1.62 | 2.06 | 1.62 | - 2.06 |
| 2.50 | 2.41 | 2.50 | - 2.41 |
| 5.00 | 3.04 | 5.00 | - 3.04 |
| 7.50 | 3.46 | 7.50 | - 3.46 |
| 10.00 | 3.76 | 10.00 | - 3.76 |
| 12.50 | 3.99 | 12.50 | - 3.99 |
| 15.00 | 4.17 | 15.00 | - 4.17 |
| 20.00 | 4.41 | 20.00 | - 4.41 |
| 25.00 | 4.56 | 25.00 | - 4.56 |
| 30.00 | 4.63 | 30.00 | - 4.63 |
| 35.00 | 4.65 | 35.00 | - 4.65 |
| 40.00 | 4.62 | 40.00 | - 4.62 |
| 45.00 | 4.56 | 45.00 | - 4.56 |
| 50.00 | 4.45 | 50.00 | - 4.43 |
| 55.00 | 4.29 | 55.00 | - 4.23 |
| 60.00 | 4.09 | 60.00 | - 3.89 |
| 65.00 | 3.84 | 62.50 | - 3.64 |
| 70.42 | 3.51 | 65.00 | - 3.31 |
| 73.94 | 3.26 | 65.83 | - 3.18 |
| 75.50 | 3.13 | 66.68 | - 3.04 |
| 77.50 | 2.96 | 69.00 | - 2.61 |
| 80.00 | 2.74 | 72.00 | - 2.09 |
| 85.00 | 2.22 | 75.50 | - 1.56 |
| 90.00 | 1.61 | 80.00 | - .99 |
| 95.00 | .87 | 85.00 | - .52 |
| 100.00 | - .02 | 90.00 | - .28 |
| | | 95.00 | - .38 |
| | | 100.00 | - 1.00 |

L. E. Radius 1.952

[redacted]

TABLE II.- STATIC PRESSURE ORIFICE LOCATIONS

[Locations given in percent airfoil chord]

On center span

| Upper surface | Lower surface |
|---|---|
| 0.00 | 0.00 |
| .62 | .65 |
| .89 | .97 |
| 1.25 | 1.45 |
| 1.86 | 2.46 |
| 2.48 | 4.96 |
| 4.98 | 7.55 |
| 7.44 | 9.99 |
| 9.94 | 12.50 |
| 12.45 | 15.01 |
| 14.97 | 20.01 |
| 19.95 | 25.03 |
| 24.95 | 30.02 |
| 29.96 | 35.00 |
| 34.97 | 39.99 |
| 39.98 | 44.97 |
| 44.99 | 50.02 |
| 50.00 | 55.02 |
| 54.98 | 59.99 |
| 60.02 | 62.50 |
| 65.00 | 64.98 |
| 70.44 | 65.81 |
| 73.97 | 66.65 |
| 75.48 | 69.00 |
| 77.45 | 71.97 |
| 79.98 | 75.53 |
| 84.96 | 80.01 |
| 89.96 | 84.96 |
| 95.03 | 89.97 |
| 100.00 (base) | 95.00 |

Spanwise (upper surface only)

| Station | Distance from center span | | | | | |
|---|---|---|---|---|---|---|
| 40.00 | -12.70 | -25.40 | -38.10 | -50.80 | -63.50 | -71.97 |
| 42.20 | 12.70 | 25.40 | 38.10 | 50.80 | 63.50 | 71.97 |
| 63.50 | 12.70 | 25.40 | 38.10 | 50.80 | 63.50 | 71.97 |
| 65.00 | -12.70 | -25.40 | -38.10 | -50.80 | -63.50 | -71.97 |
| 90.00 | 12.70 | 25.40 | 38.10 | 50.80 | 63.50 | 71.97 |
| 90.00 | -12.70 | -25.40 | -38.10 | -50.80 | -63.50 | -71.97 |



[redacted]

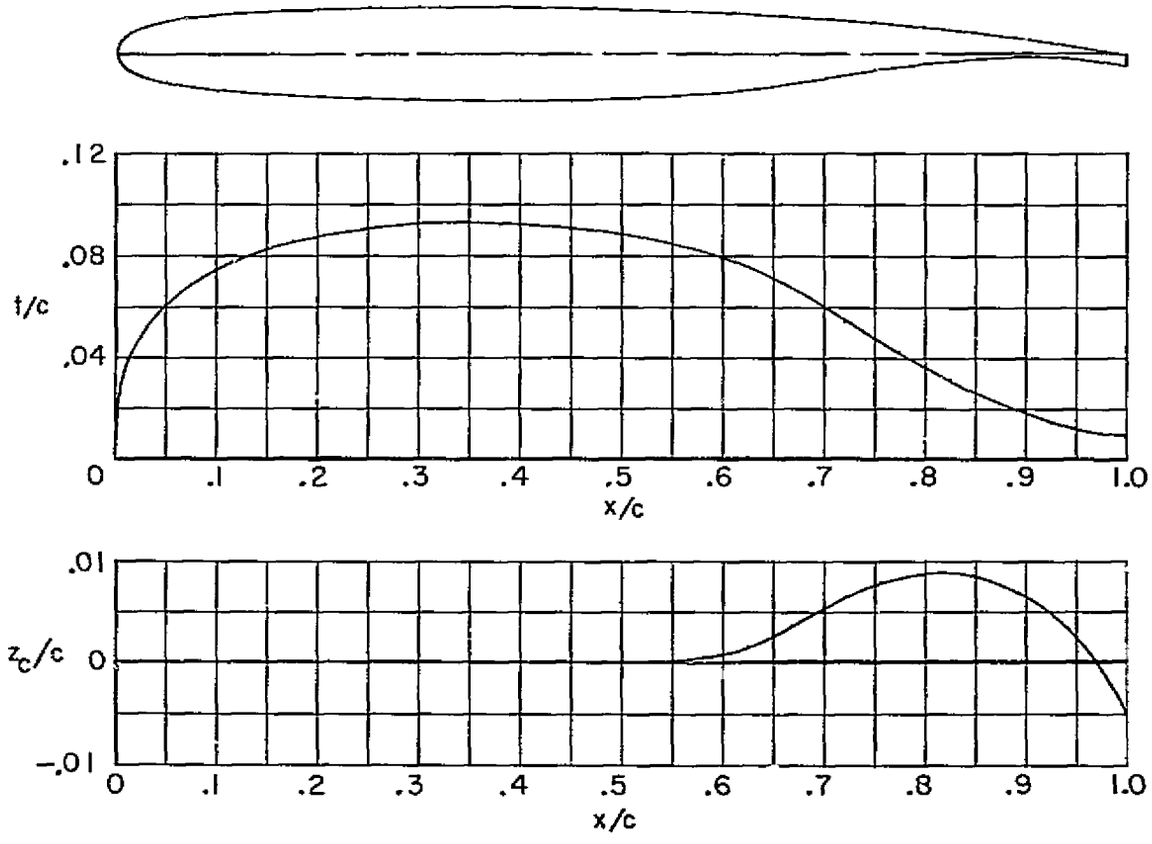


Figure 1.- Profile, thickness distribution, and camber line of the 9.3-percent-thick supercritical airfoil.

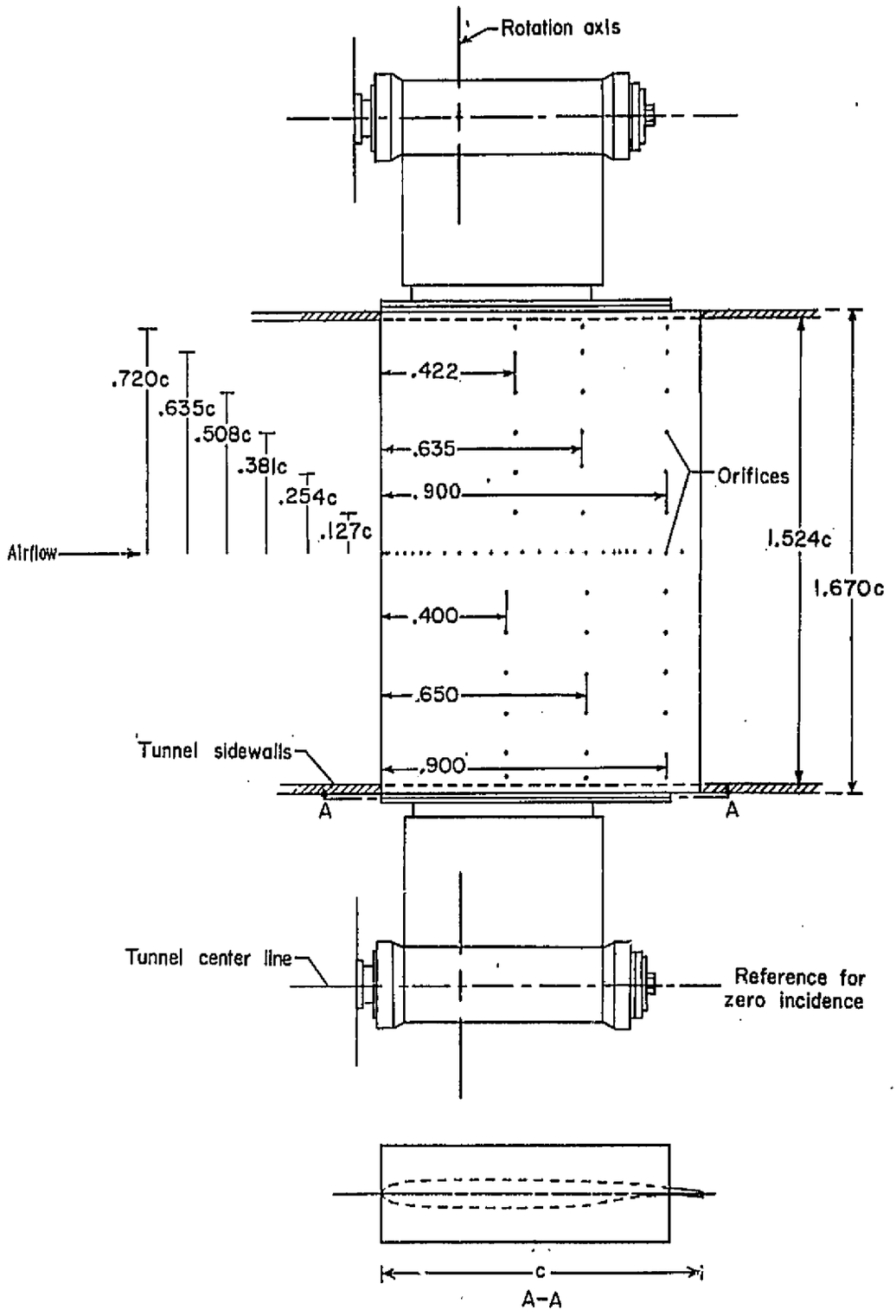


Figure 2.- Installation of the airfoil in the wind tunnel. All dimensions are in terms of airfoil chord. c = 0.6 m (23.622 in.)

NASA
L-71-5286

Figure 3.- Typical photograph of an airfoil mounted in the wind tunnel.

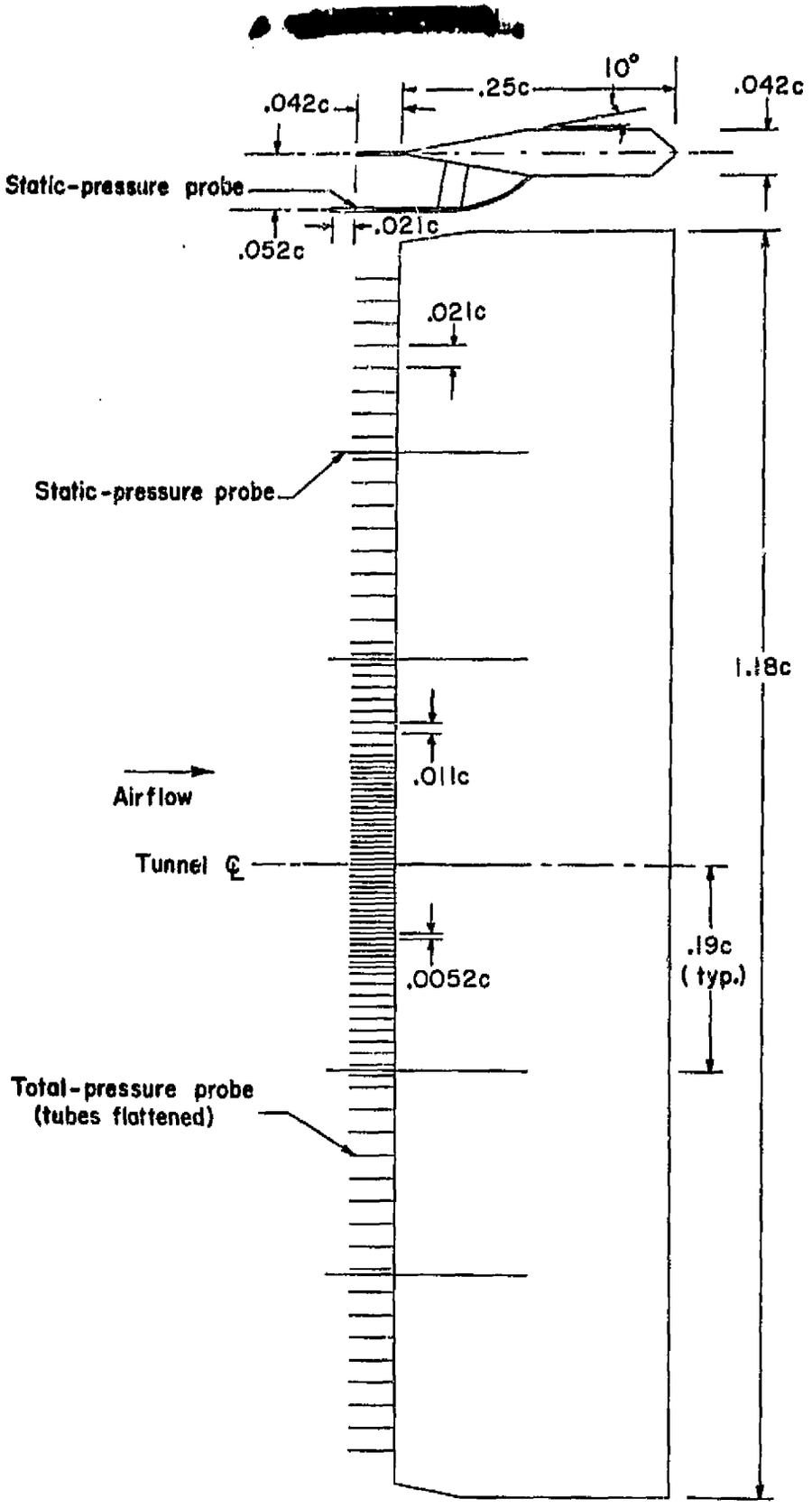


Figure 4.- Drawing of wake rake. All dimensions in terms of airfoil chord. c = 0.6 m (23.622 in.)

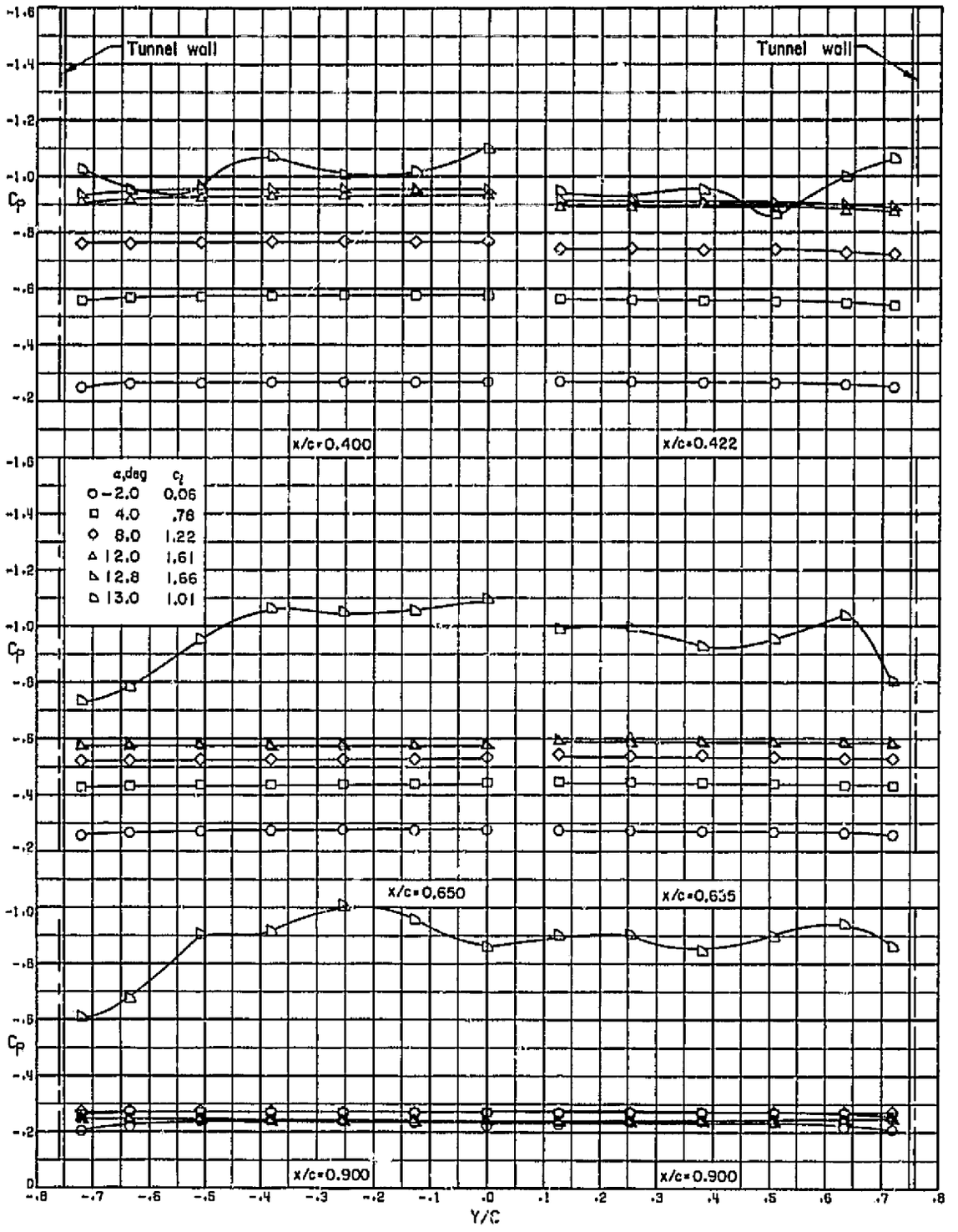


(a) R = 2.9 x $10^6$.

Figure 5.- Effect of angle of attack and Reynolds number on the upper surface spanwise pressure distributions. M = 0.20.

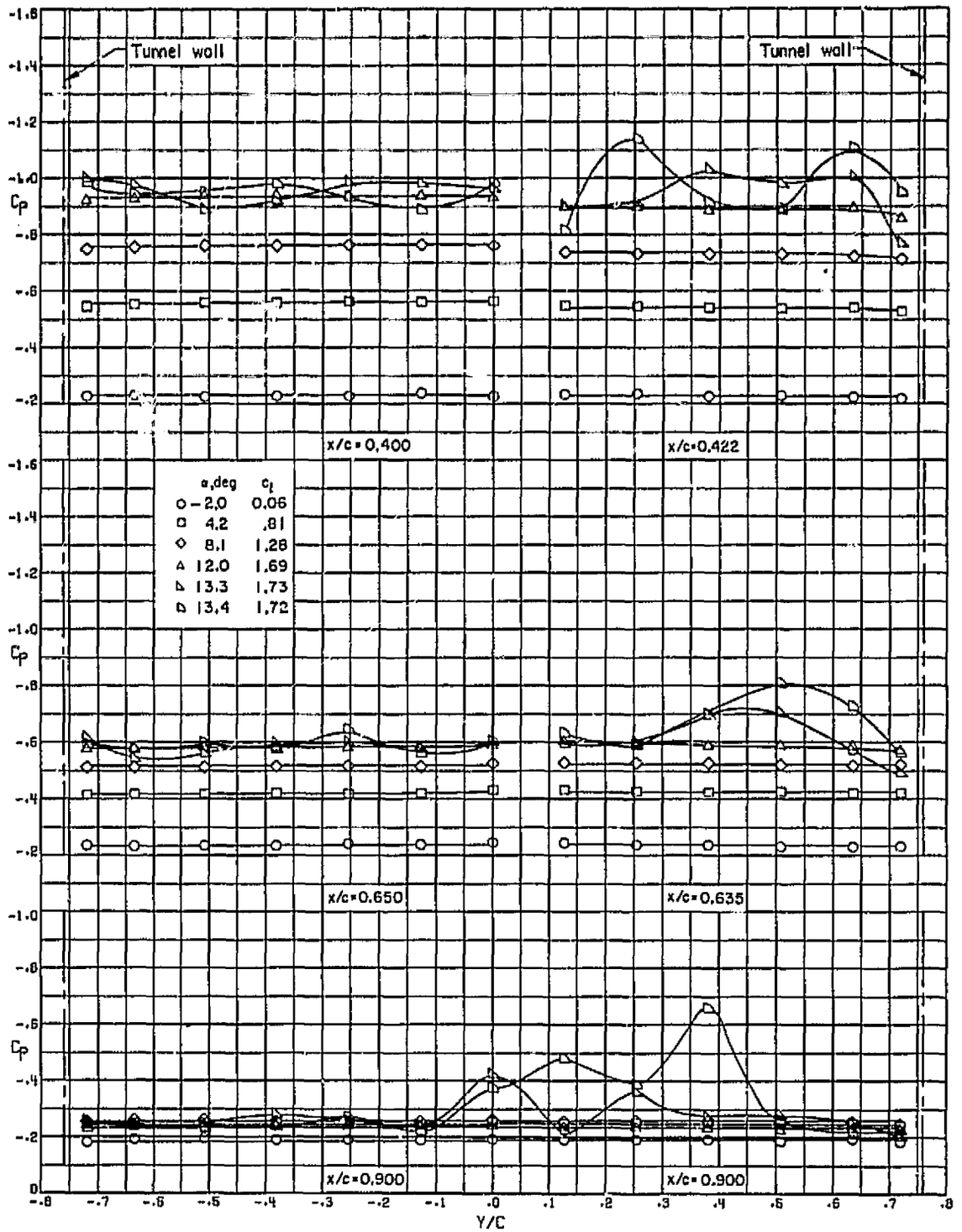


(b) $R = 8.8 \times 10^6$.

Figure 5.- Continued.

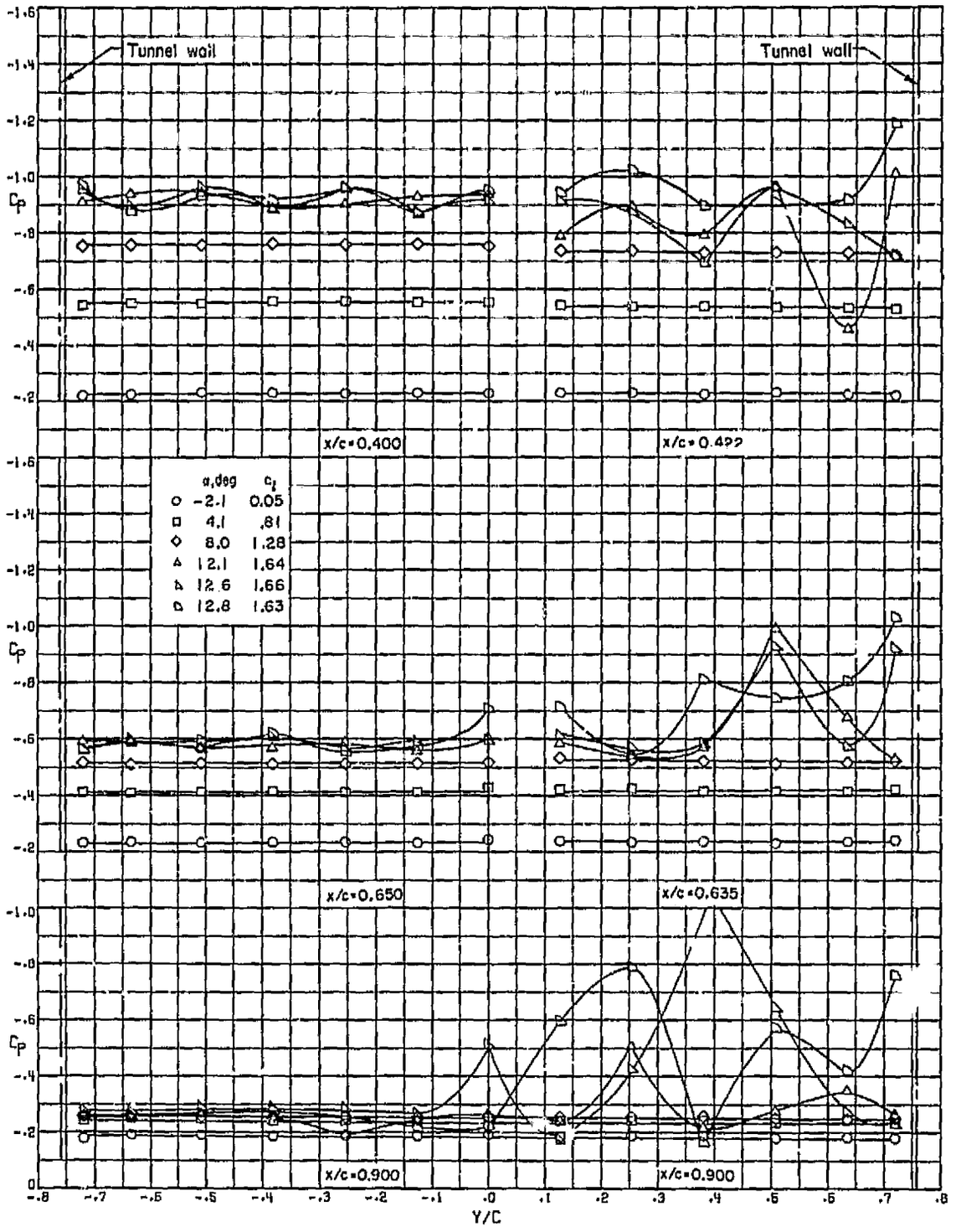


(c) $R = 16.8 \times 10^6$.

Figure 5.- Concluded.

Figure 6. - Tuft photographs of the effect of angle of attack on the upper surface flow pattern. $R = 8.8 \times 10^6$; $M = 0.20$.

Figure 6.- Concluded.

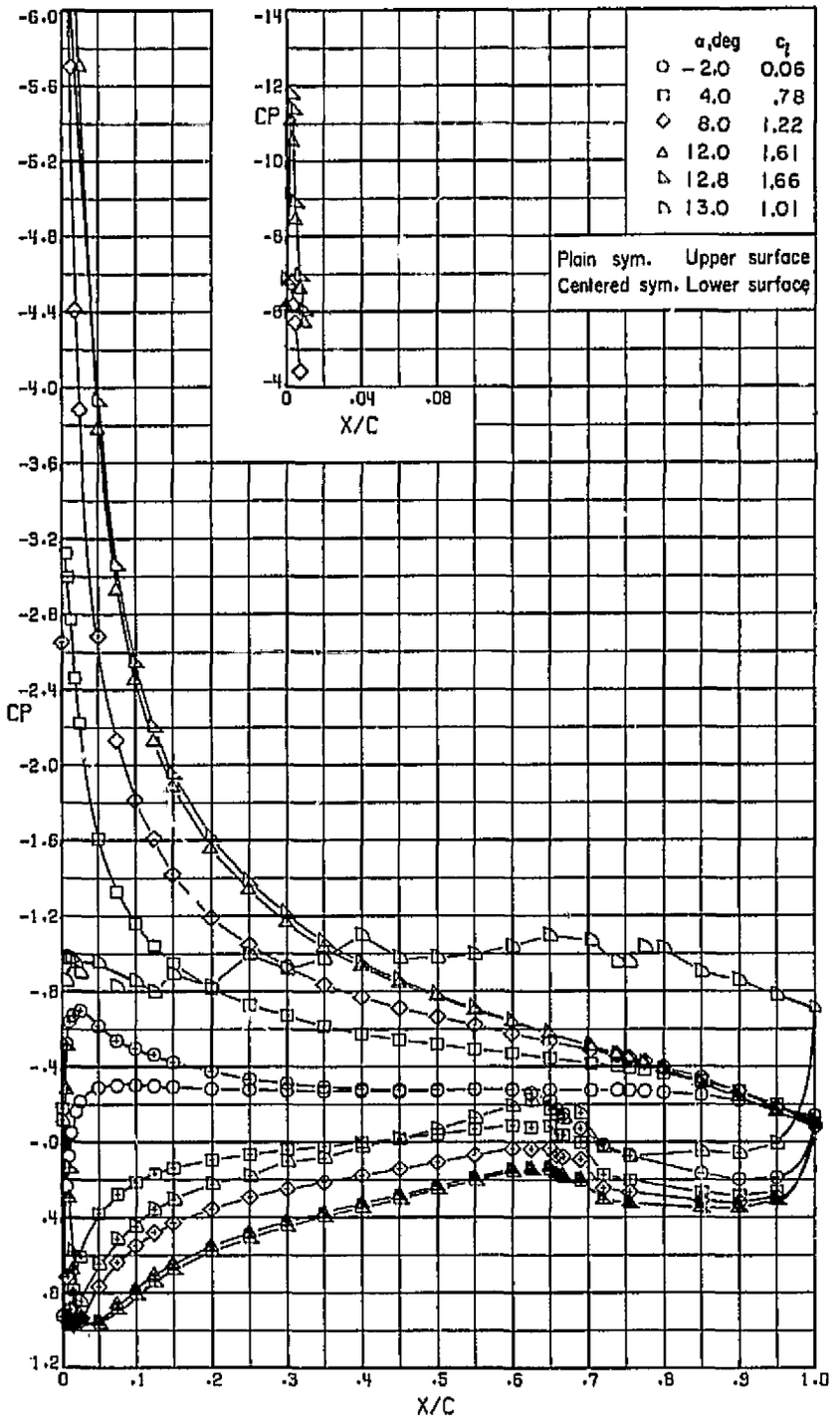


(a) $R = 2.9 \times 10^6$.

Figure 7.- Effect of angle of attack and Reynolds number on the chordwise pressure distribution. $M = 0.20$.

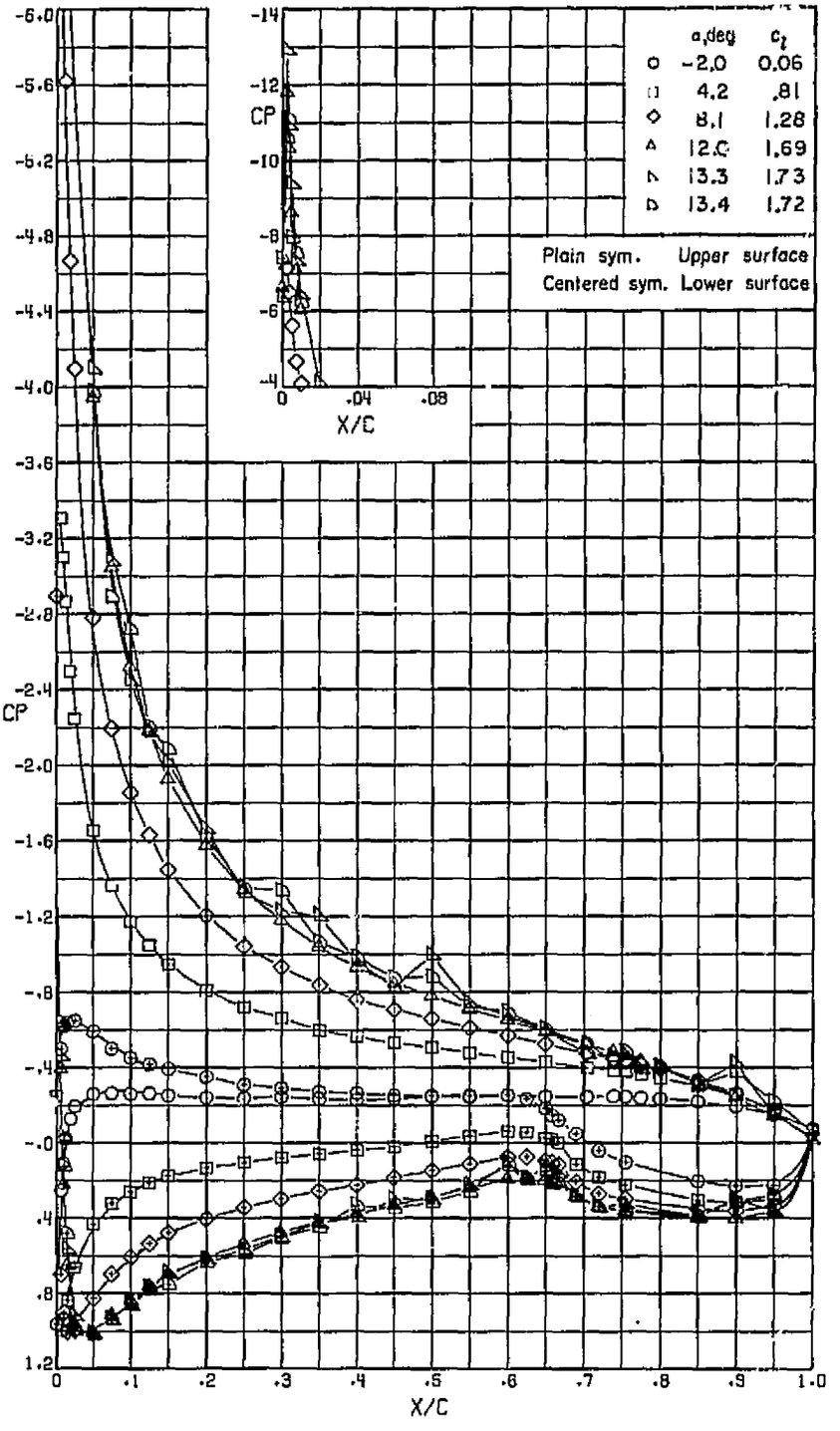


(b) R = 8.8 x $10^6$.

Figure 7.- Continued.

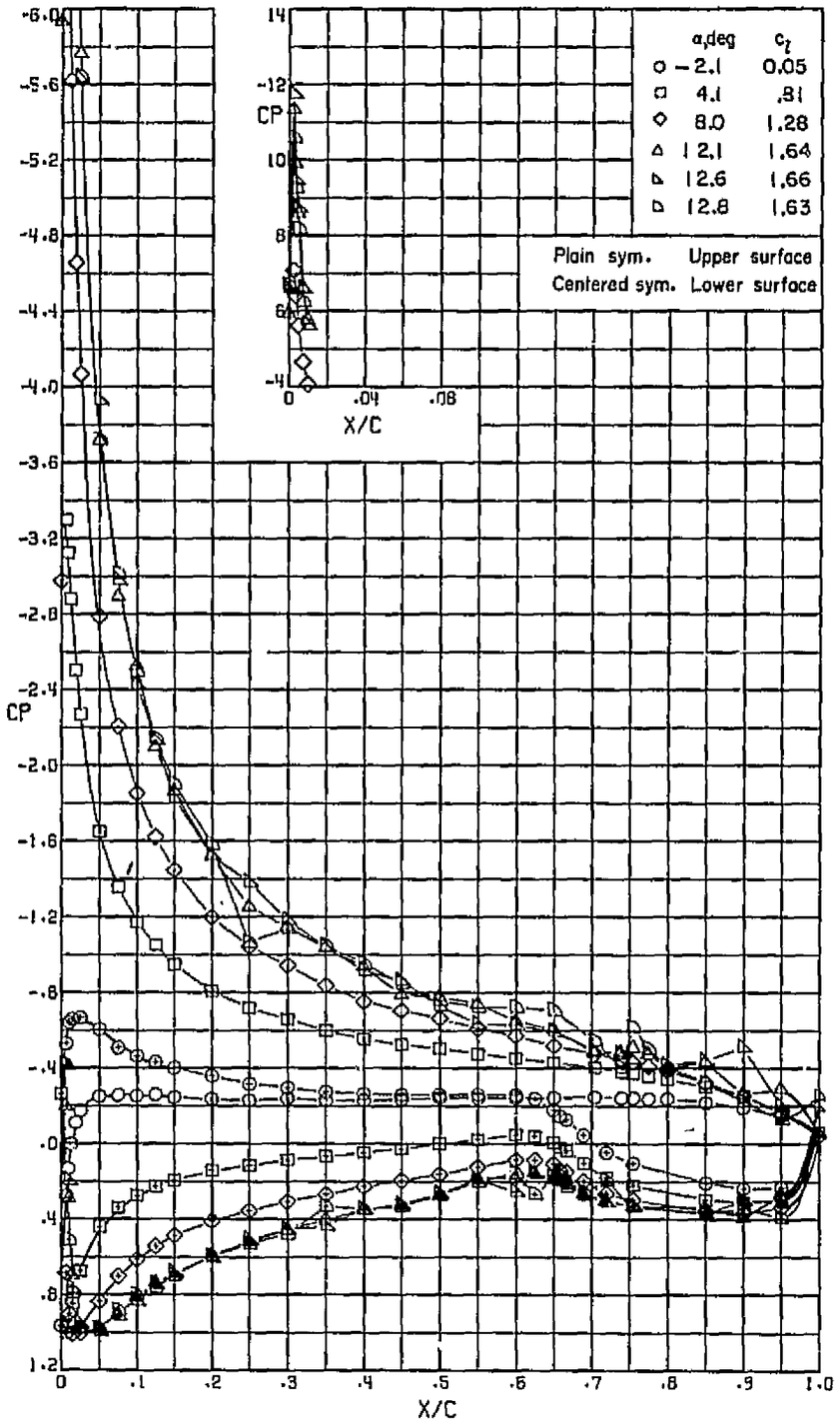


(c) R = 16.8 x $10^6$.

Figure 7.- Concluded.

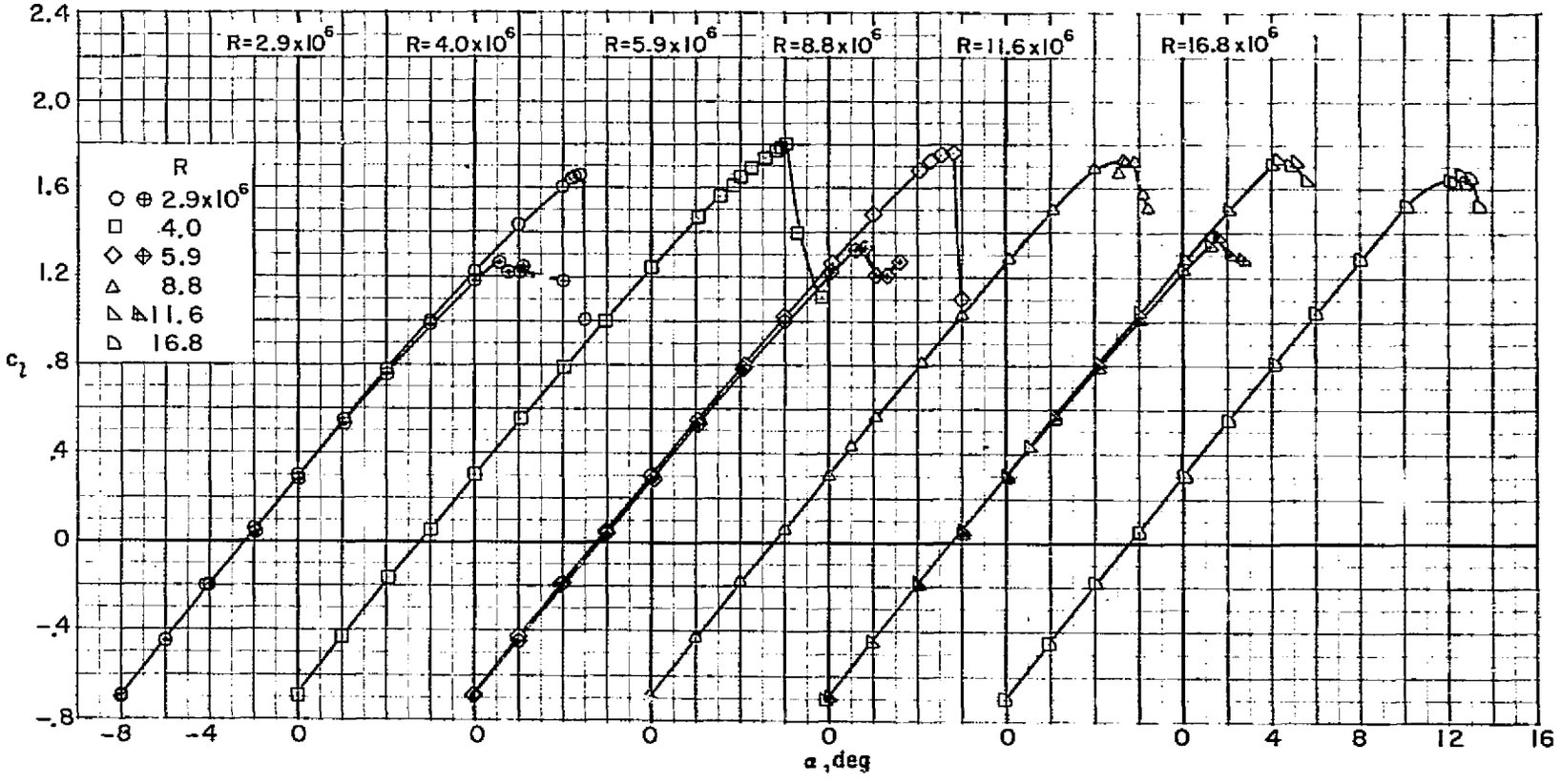


(a) Effect of Reynolds number, M = 0.20.

Figure 8.- Section lift characteristics of the 9.3-percent-thick supercritical airfoil. Plain symbols indicate airfoil with smooth surface; centered symbols, NACA standard roughness.

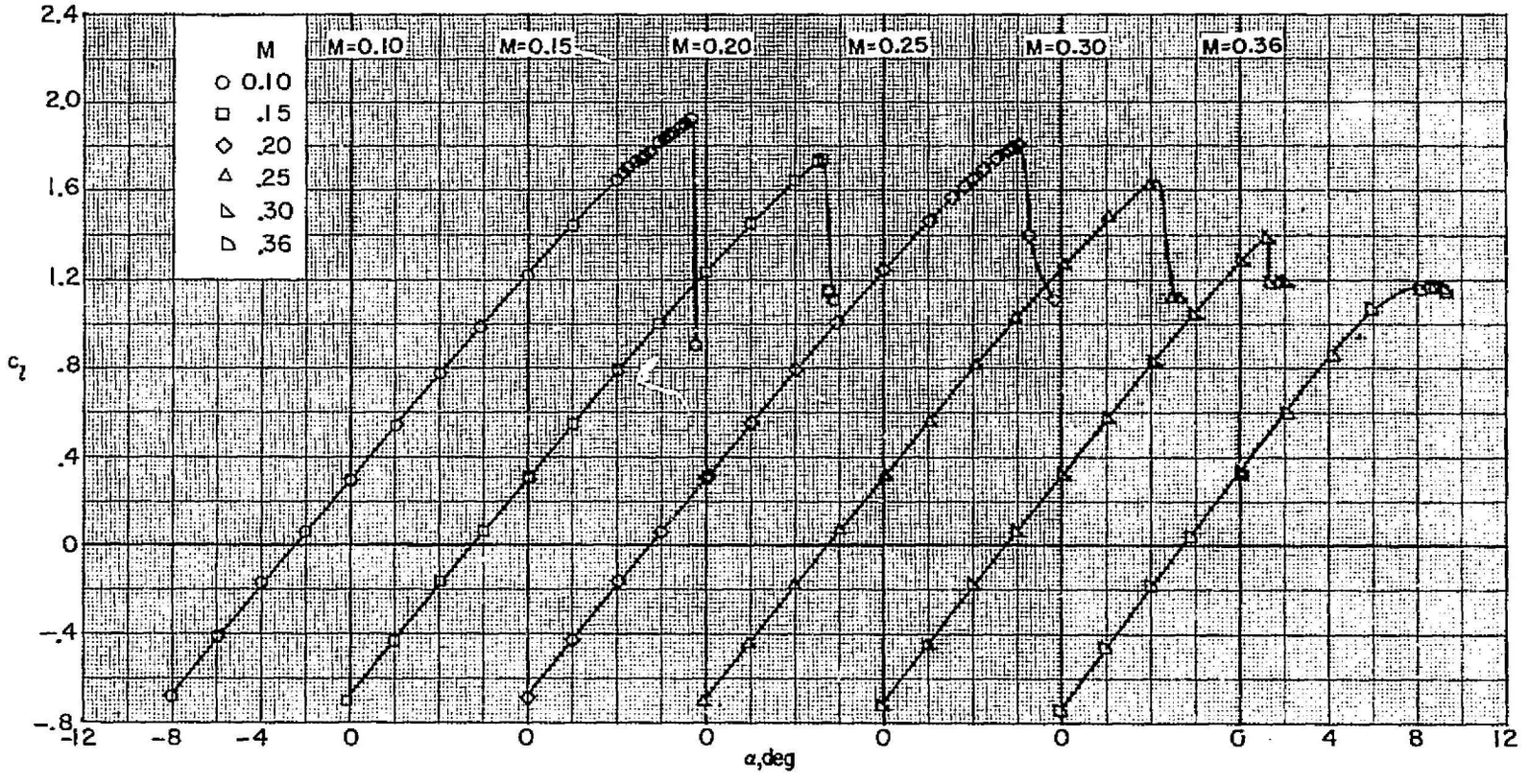


(b) Effect of Mach number, $R = 4.0 \times 10^6$.

Figure 8.- Concluded.

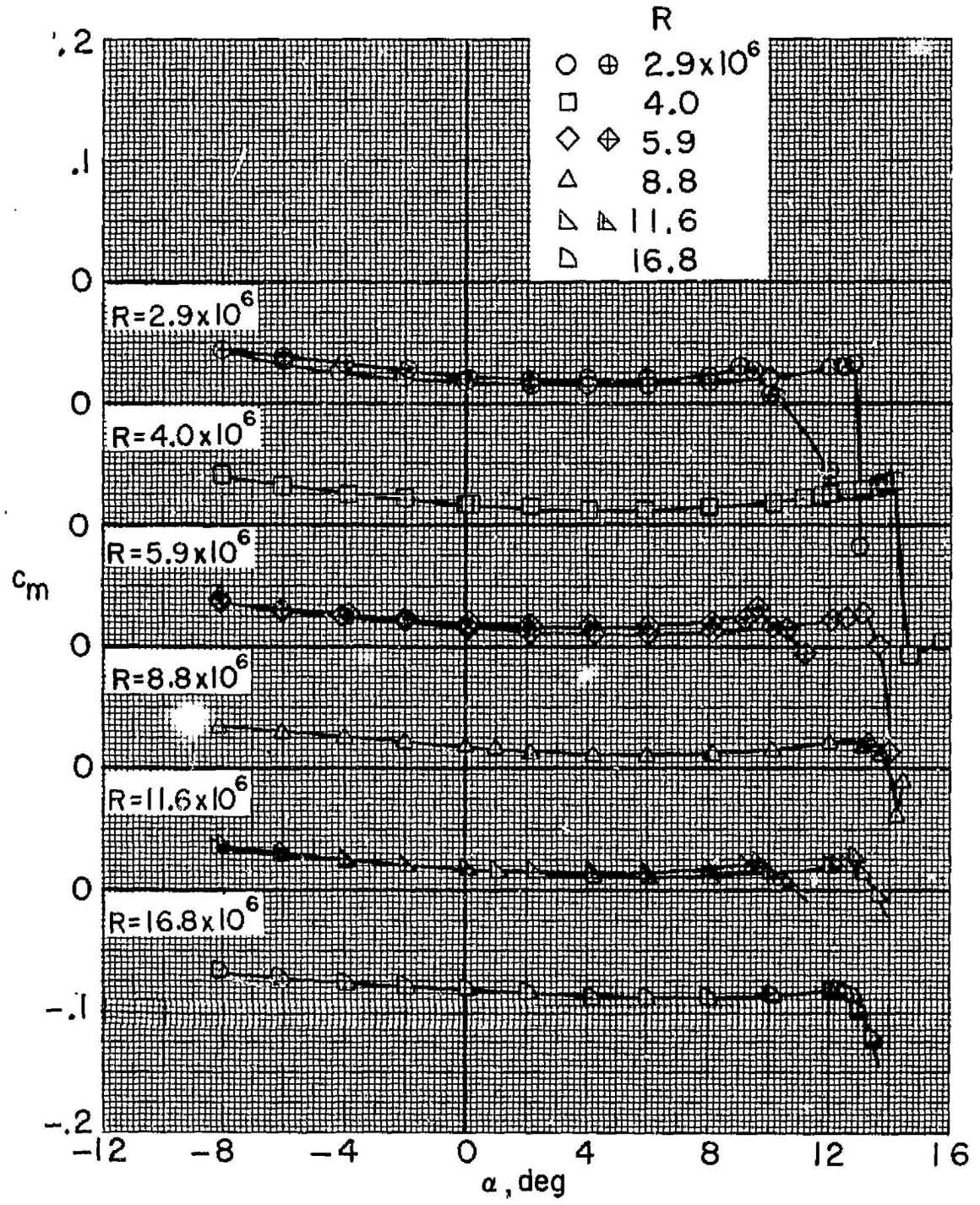


(a) Effect of Reynolds number, M = 0.20.

Figure 9.- Section pitching-moment characteristics of the 9.3-percent thick supercritical airfoil. Plain symbols indicate airfoil with smooth surface; centered symbols, NACA standard roughness.

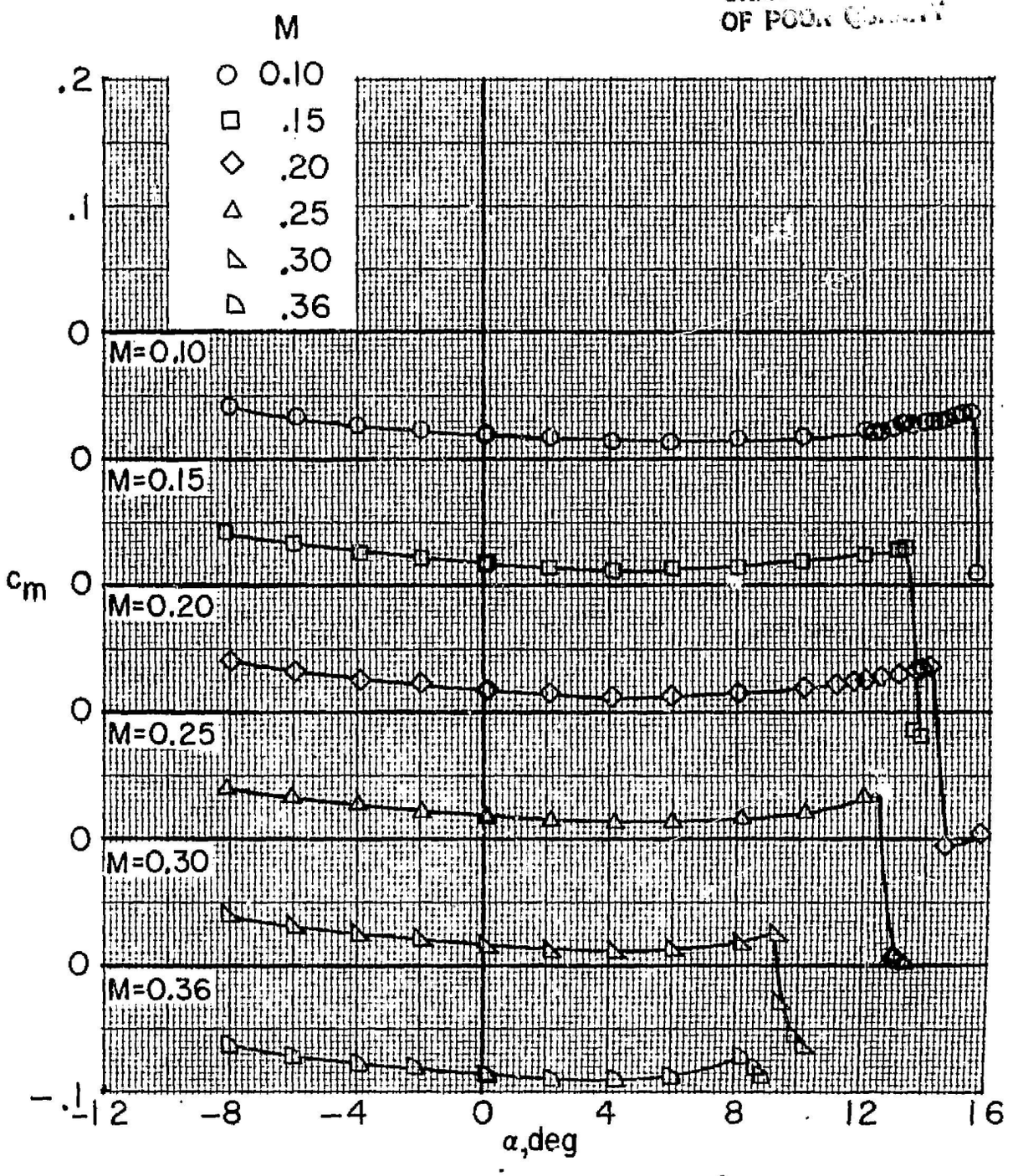


(b) Effect of Mach number, R = 4.0 x $10^6$.

Figure 9.- Concluded.

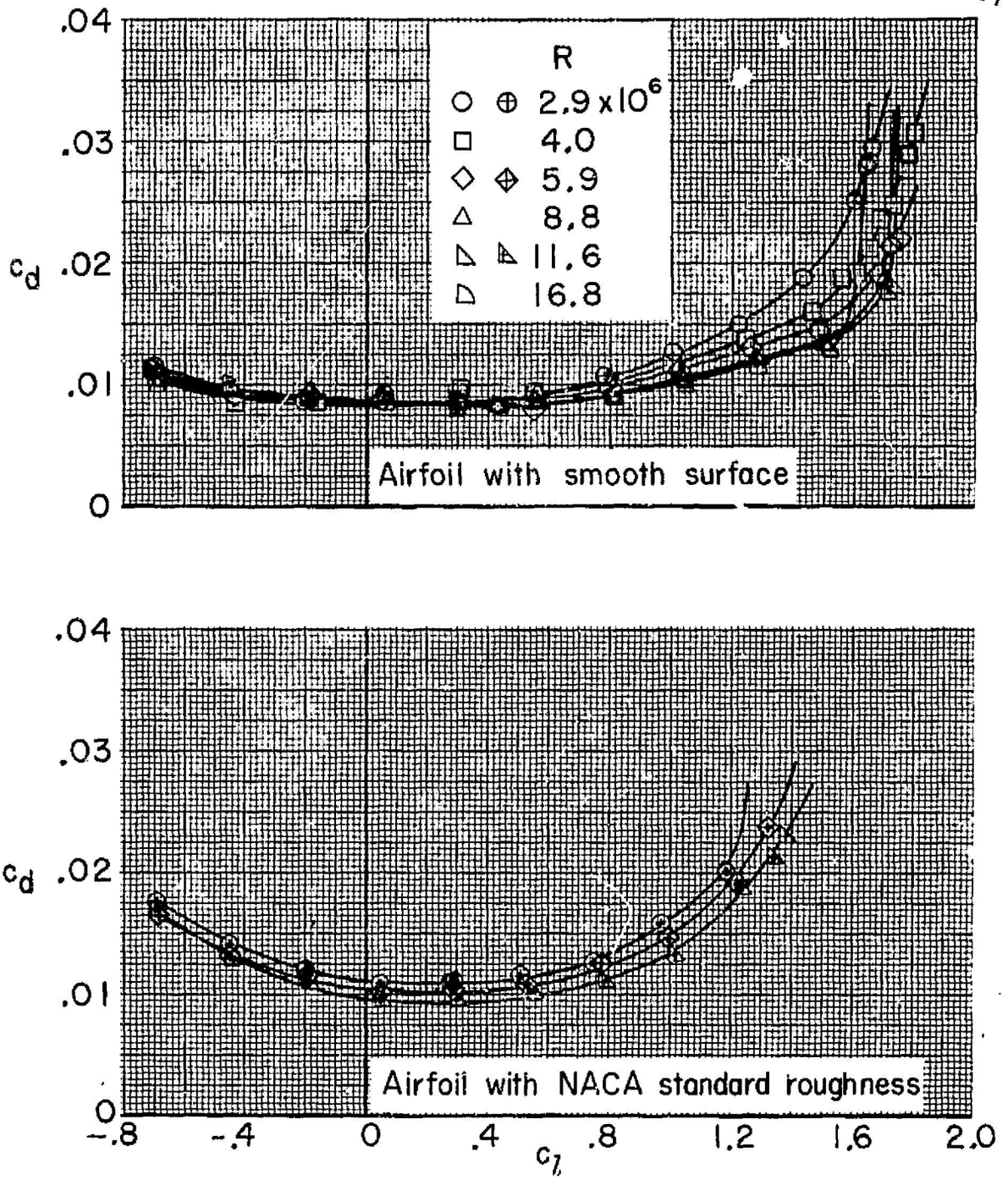


(a) Effect of Reynolds number. M = 0.20.

Figure 10.- Section drag characteristics of the 9.3-percent-thick supercritical airfoil. Plain symbols indicate airfoil with smooth surface; centered symbols, NACA standard roughness.

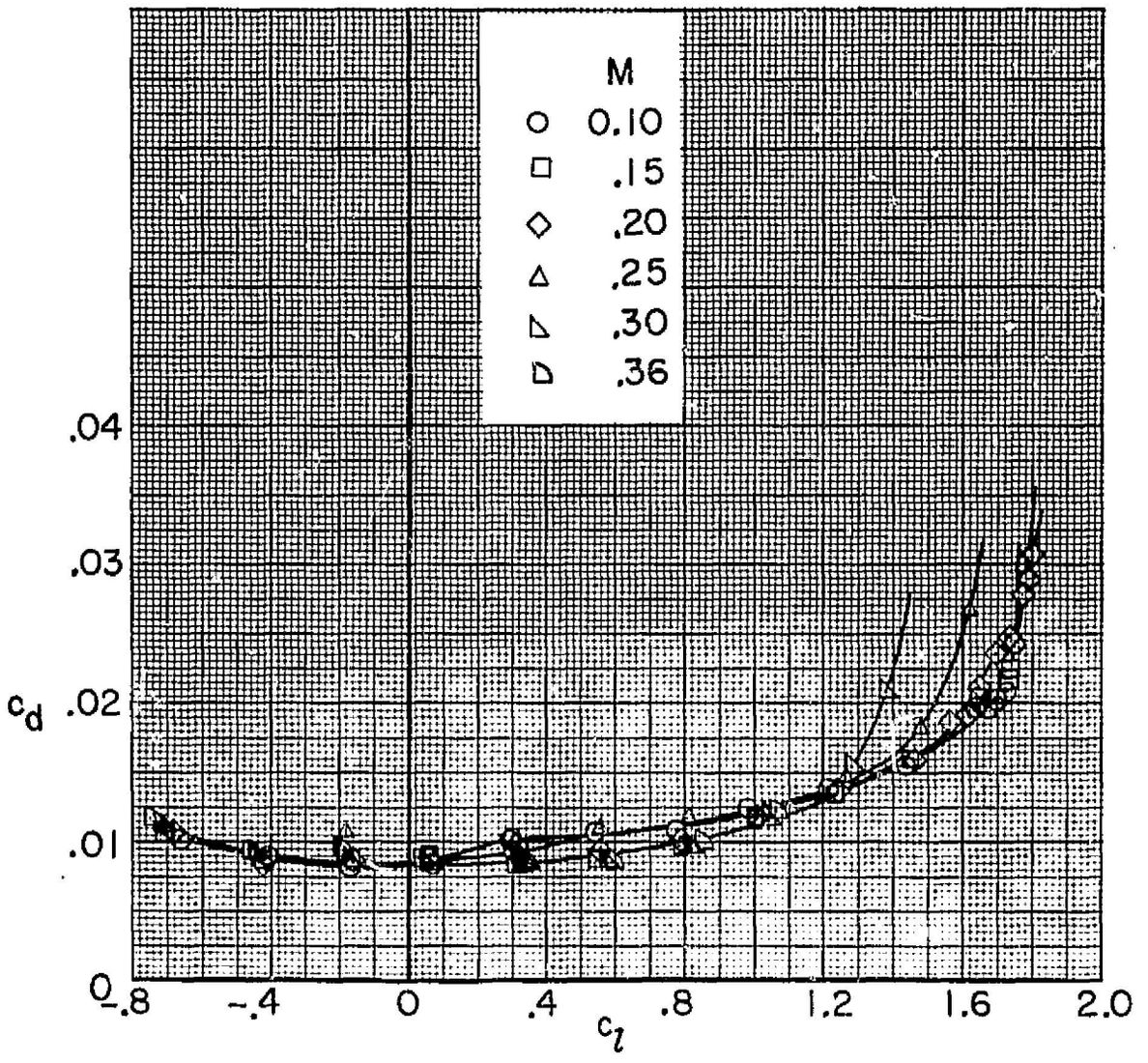


(b) Effect of Mach number. $R = 4.0 \times 10^6$.

Figure 10.- Concluded.

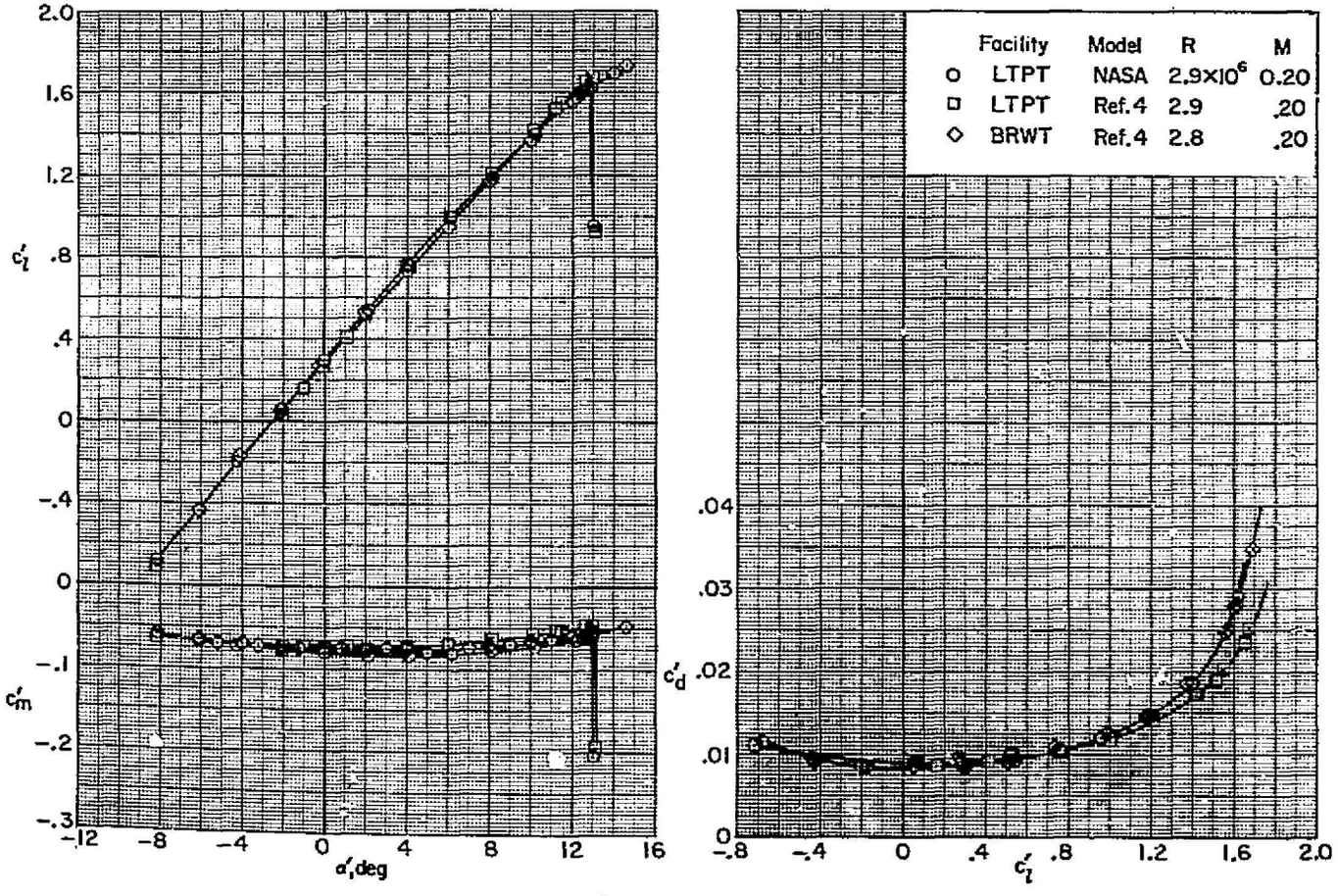


Figure 11.- Comparison of section coefficients with the data of ref. 4.

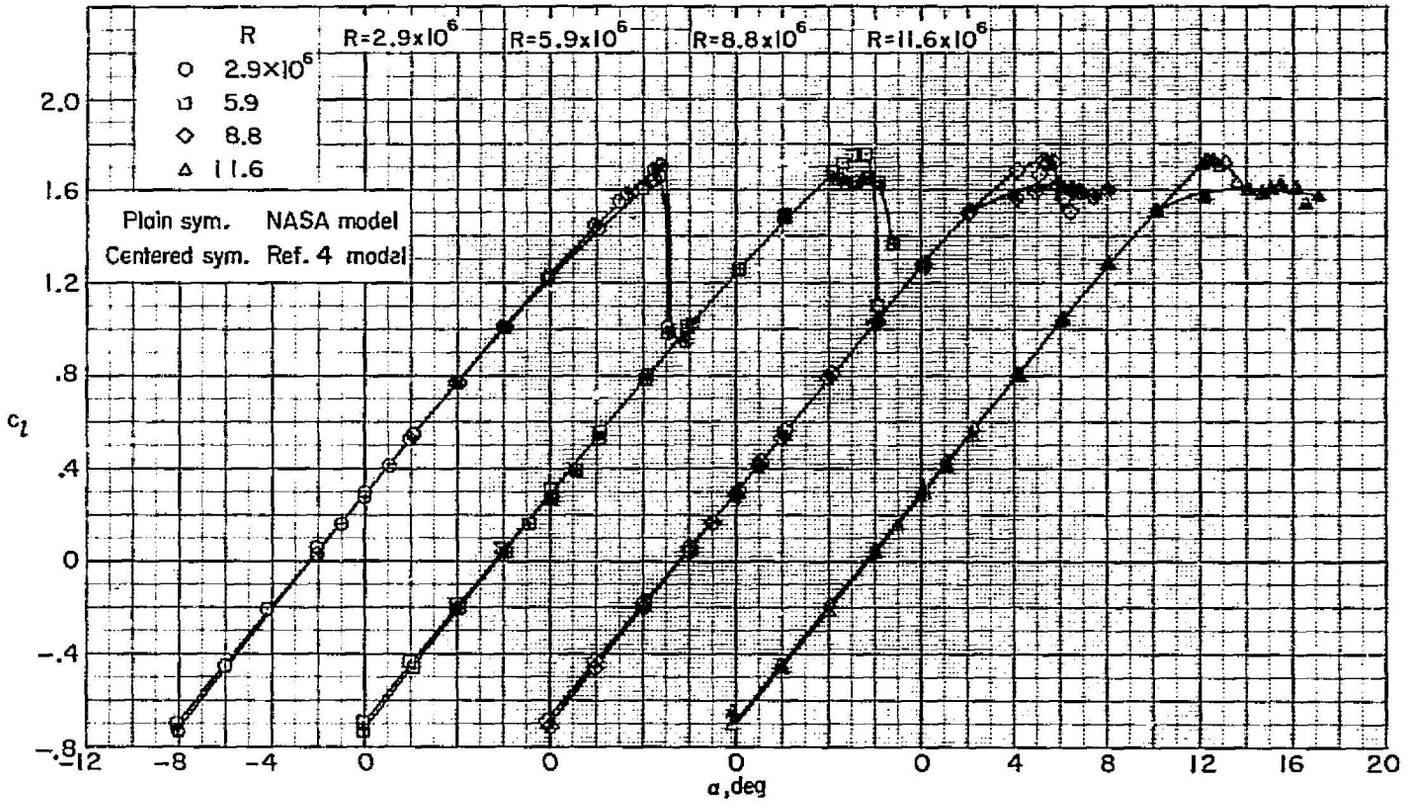


(a) Section lift characteristics.

Figure 12.- Comparison of section coefficients on the NASA model and the model of ref. 4. M = 0.20.

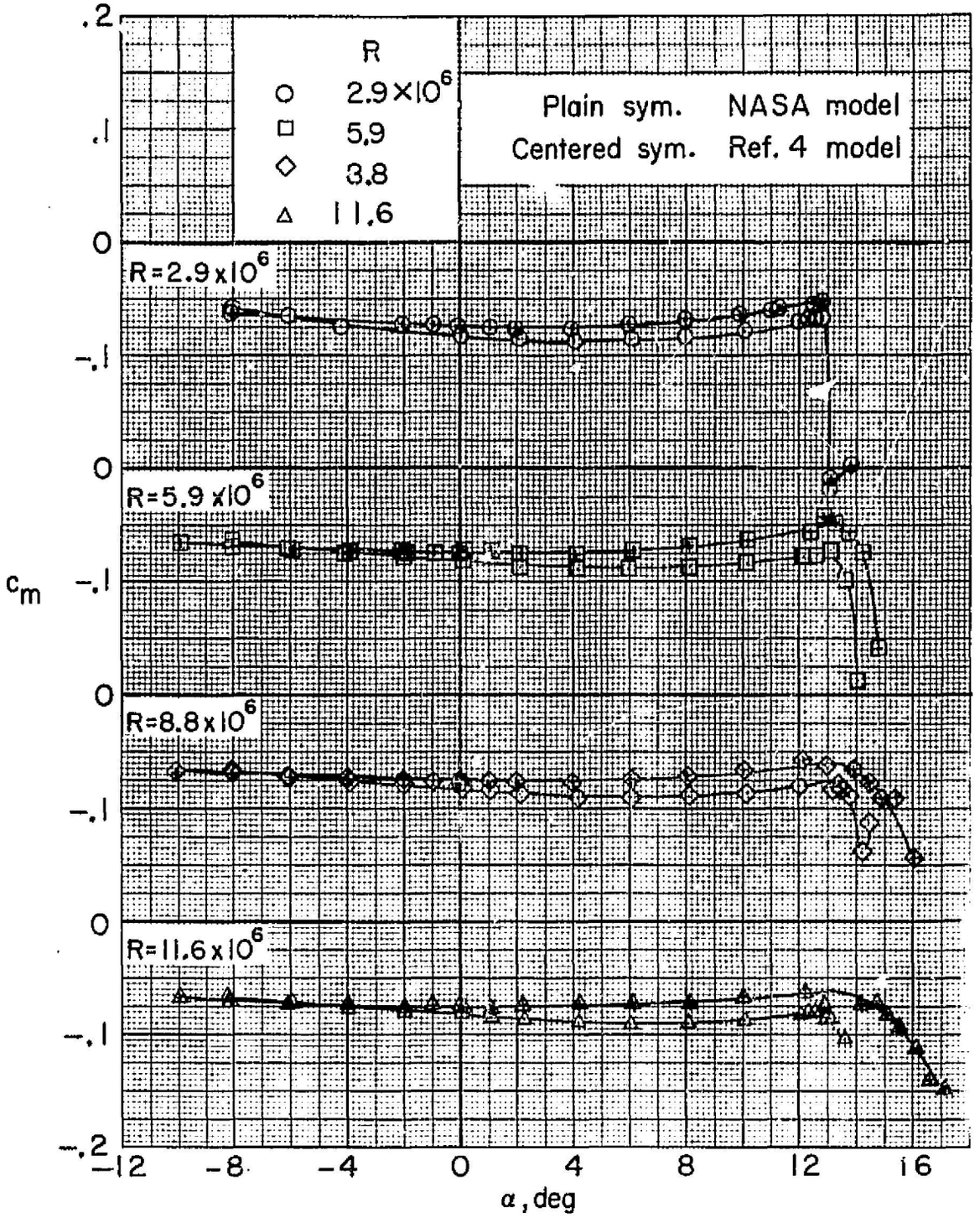


(b) Section pitching-moment characteristics.

Figure 12. - Continued.

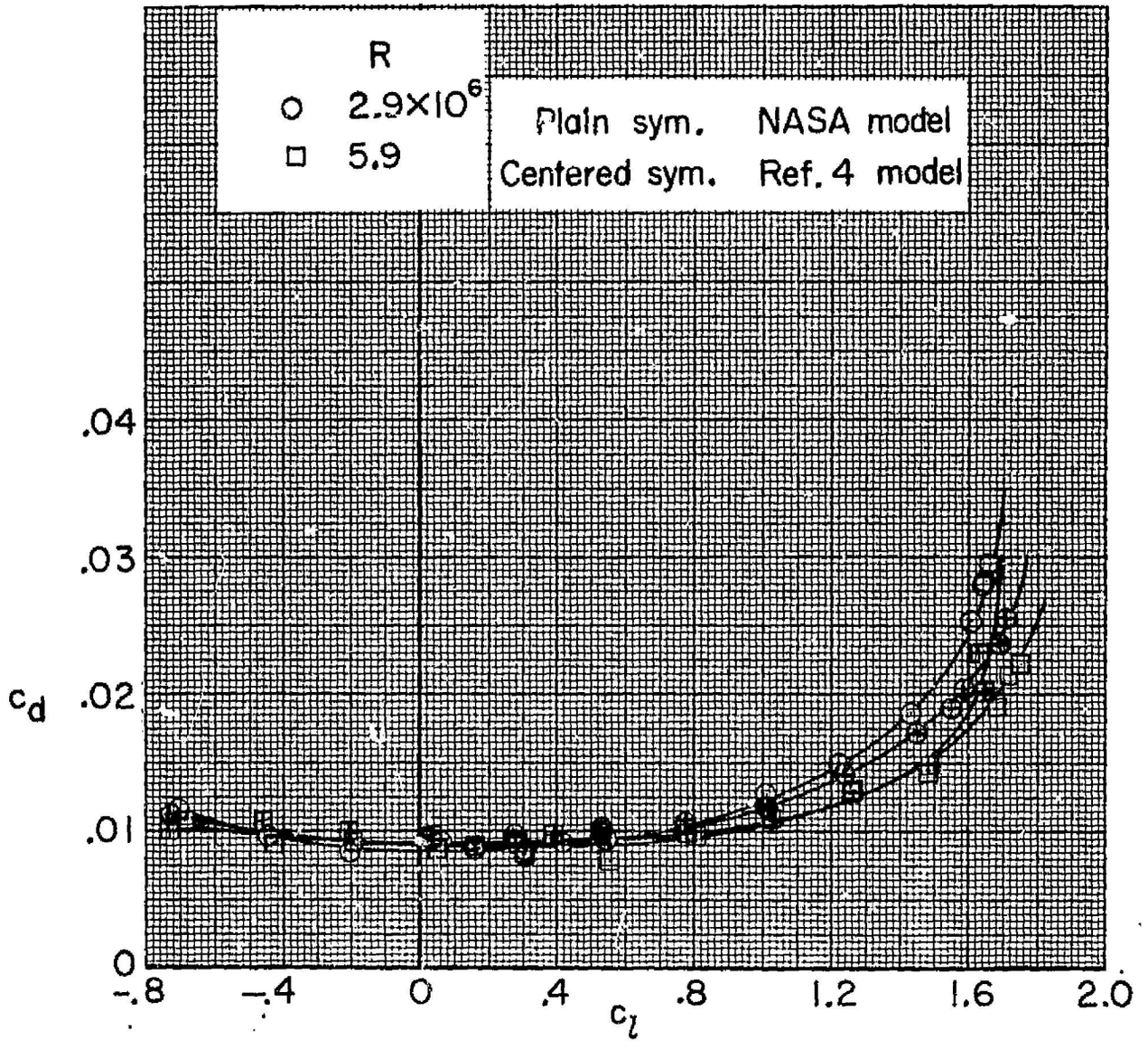


(c) Section drag characteristics.

Figure 12.- Continued.

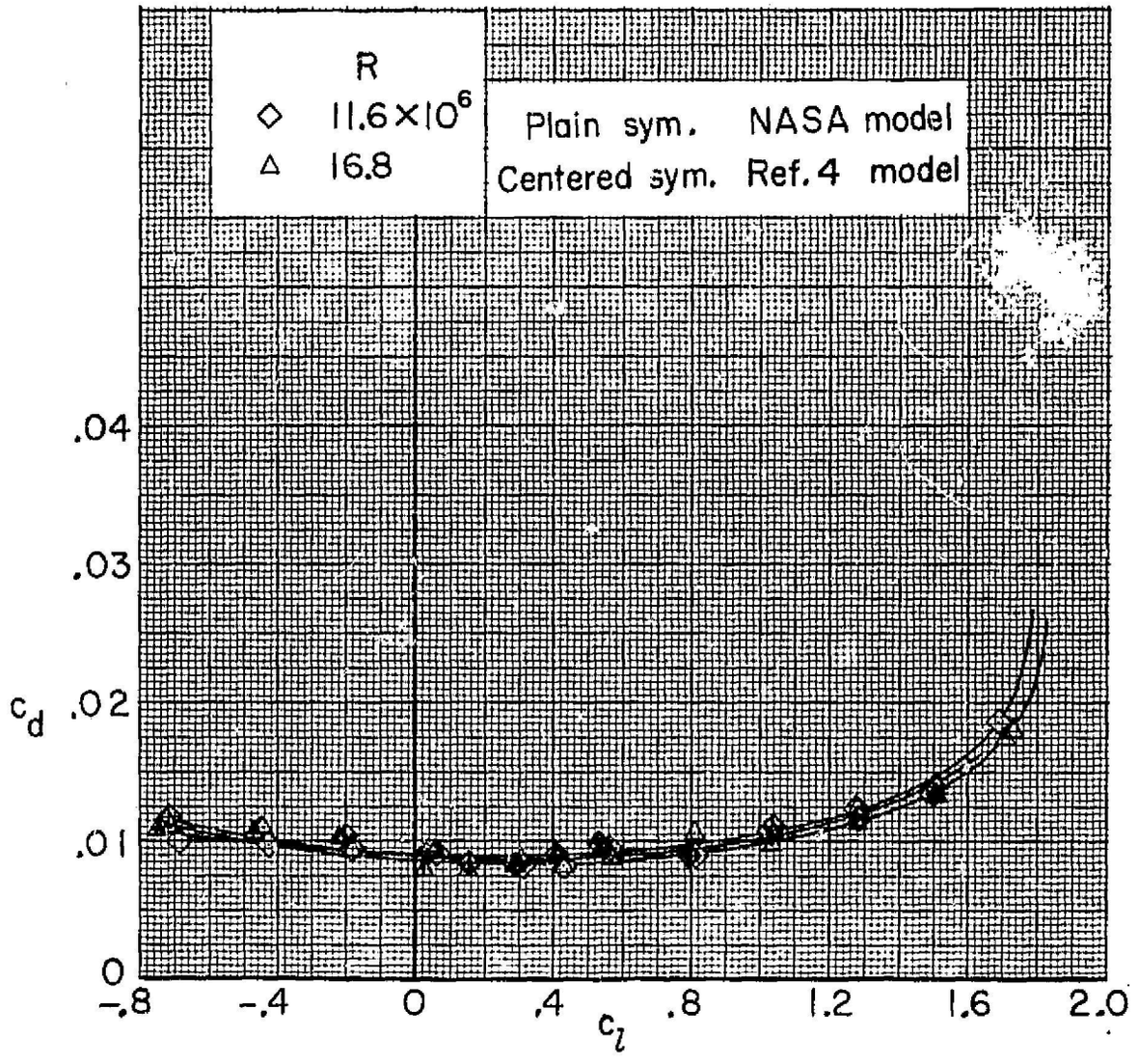


(d) Section drag characteristics.

Figure 12.- Concluded.

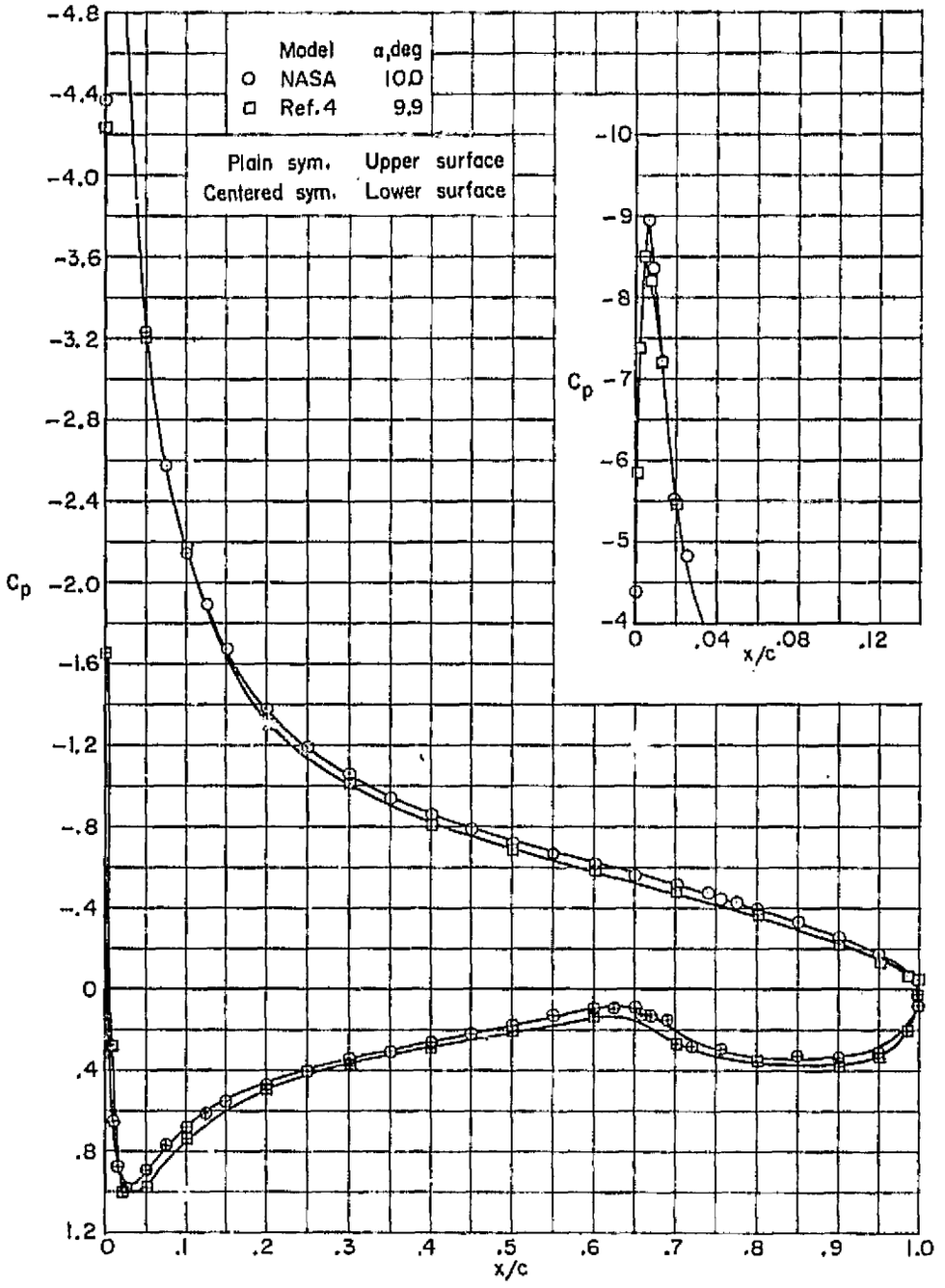


(a) $R = 2.9 \times 10^6$.

Figure 13. - Comparison of chordwise pressure distributions on the NASA model and the model of ref. 4. M = 0.20.

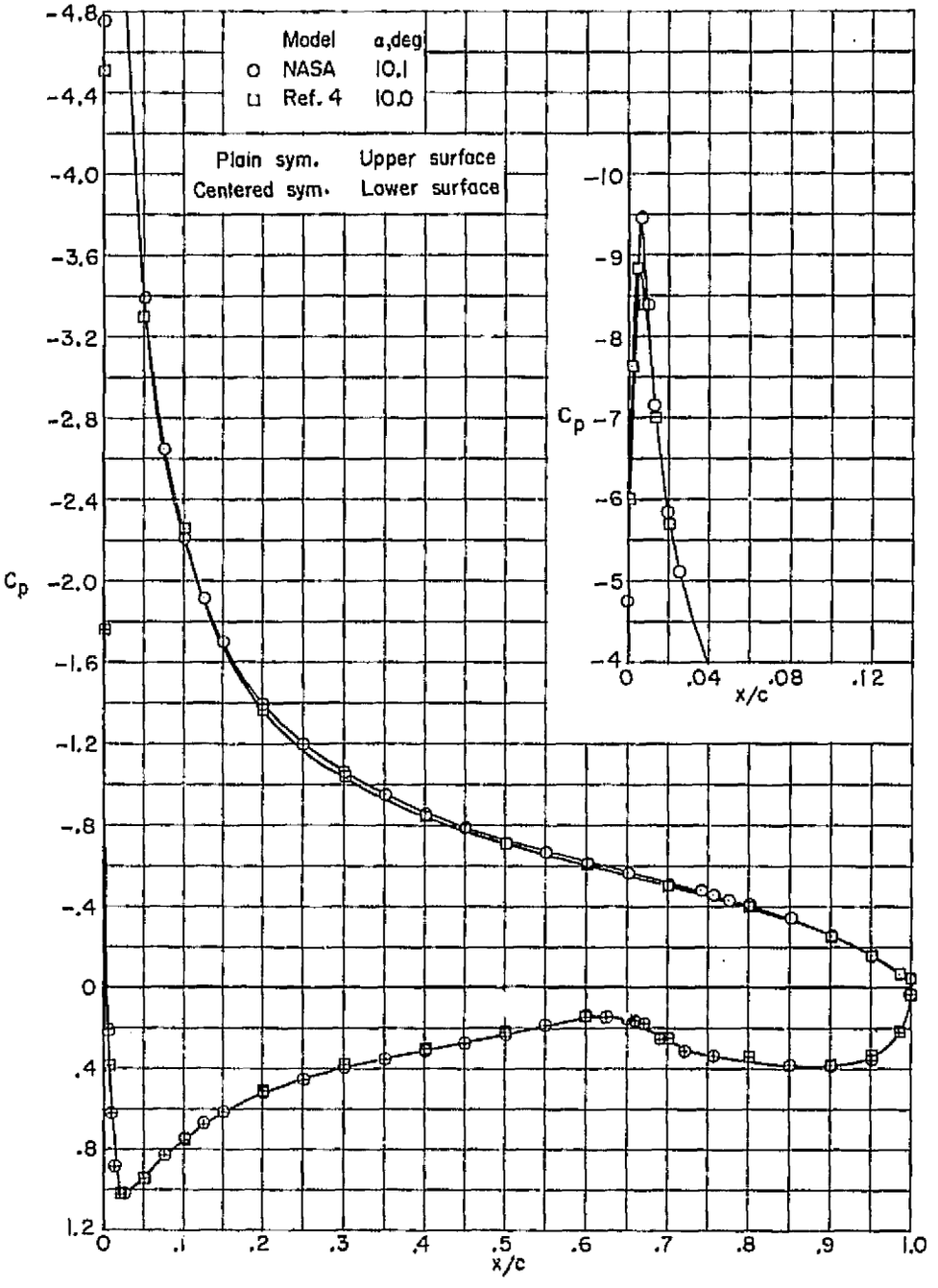


(b) $R = 11.6 \times 10^6$.

Figure 13.- Concluded.

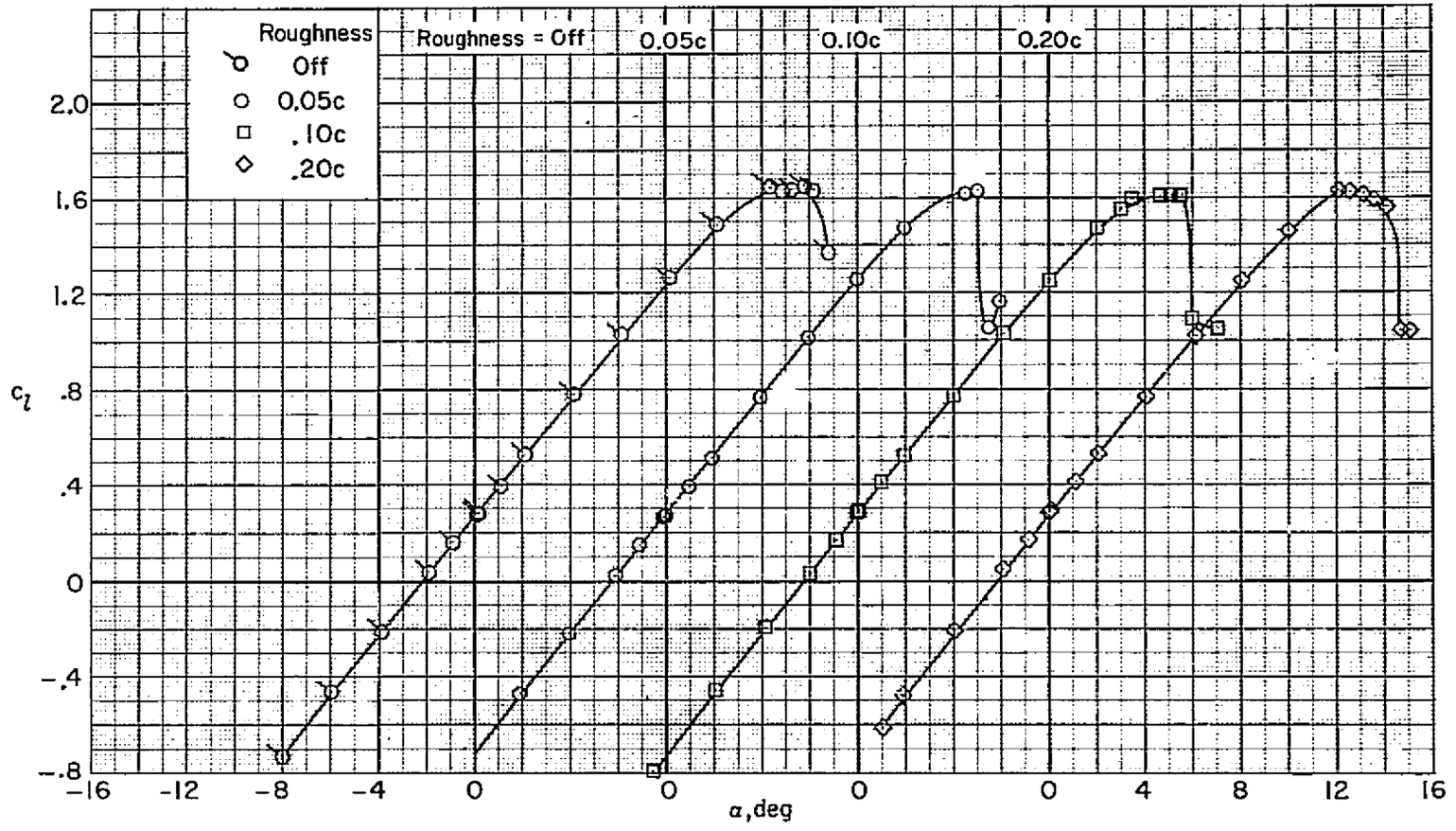


(a) Section lift characteristics.

Figure 14.- Effect of roughness location on the aerodynamic characteristics of the 9.3-percent-thick supercritical airfoil. Ref. 4 model; R = 5.9 x $10^6$; M = 0.20.

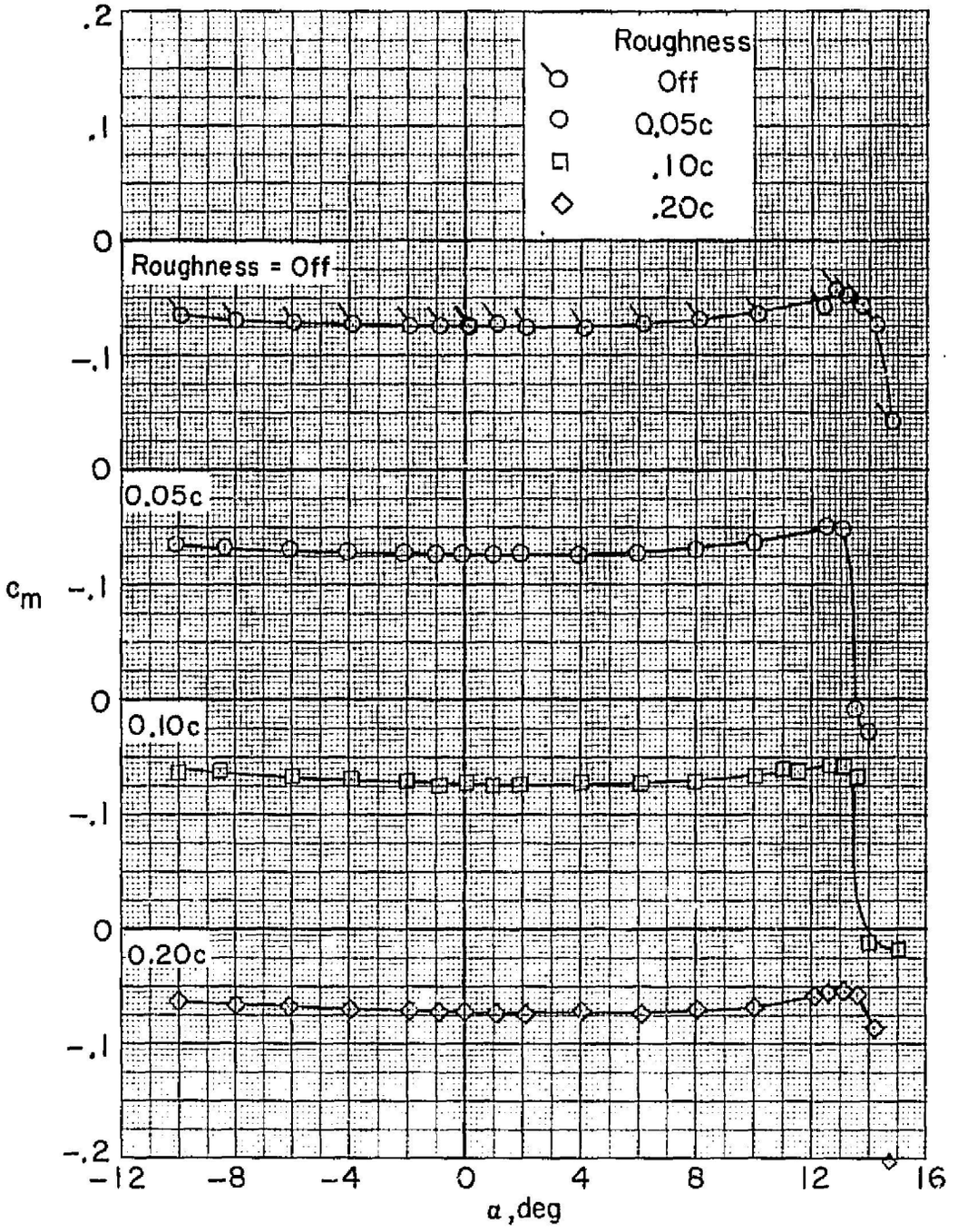


(b) Section pitching-moment characteristics.

Figure 14.- Continued.

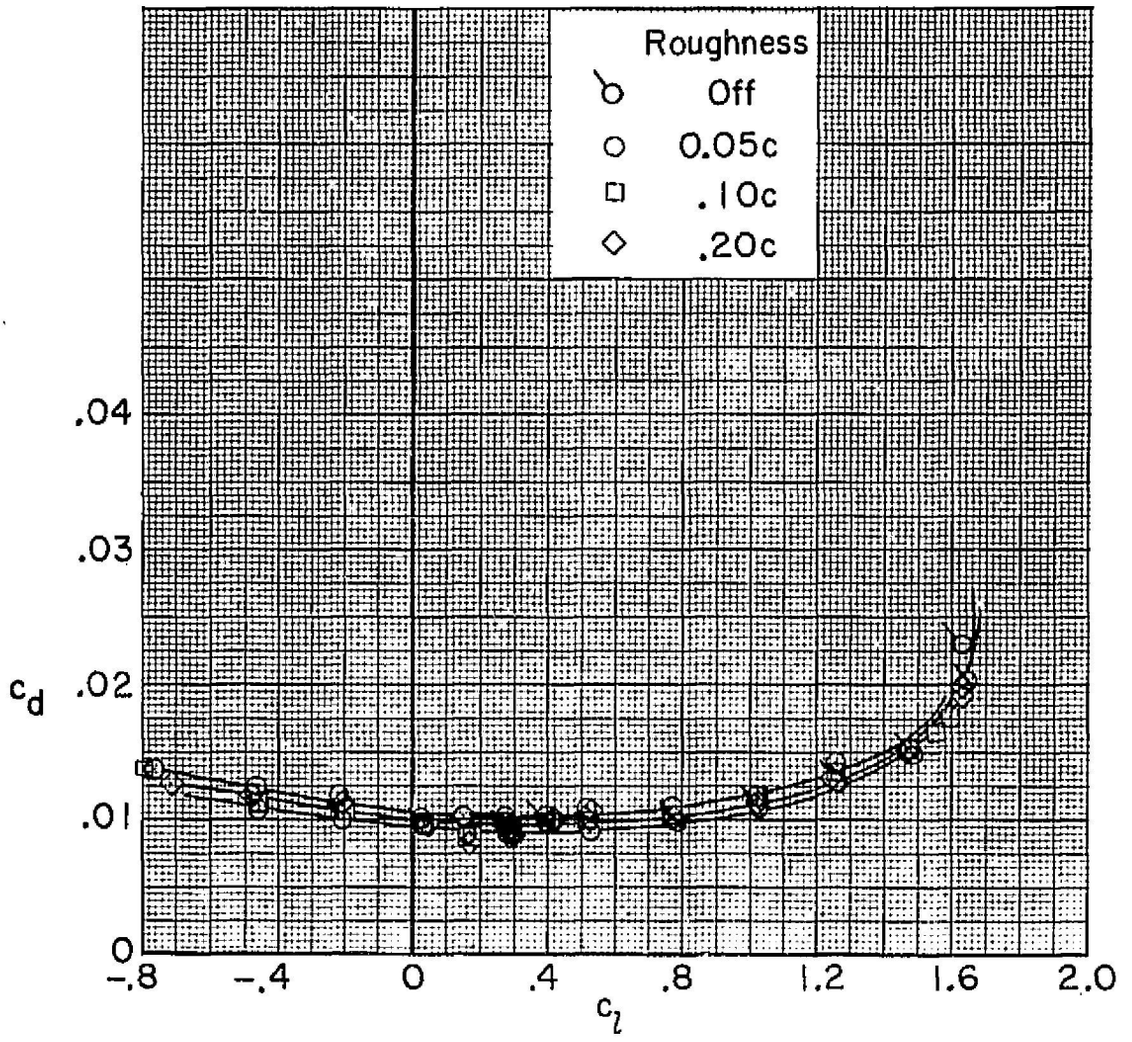


(c) Section drag characteristics.

Figure 14.- Concluded.

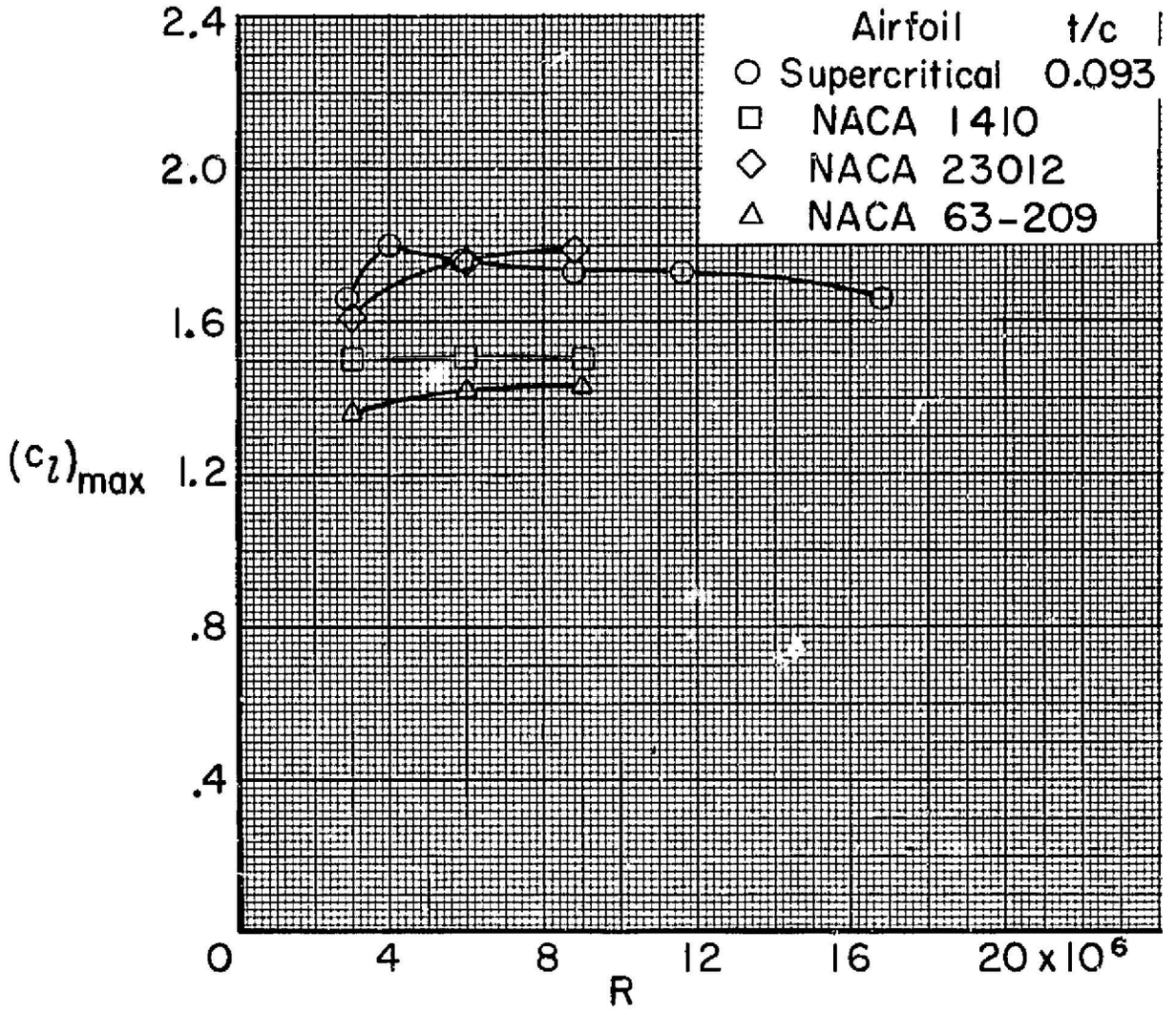


Figure 15.- Comparison of the 9.3-percent-thick supercritical airfoil with some conventional airfoils. $M \leq 0.20$.

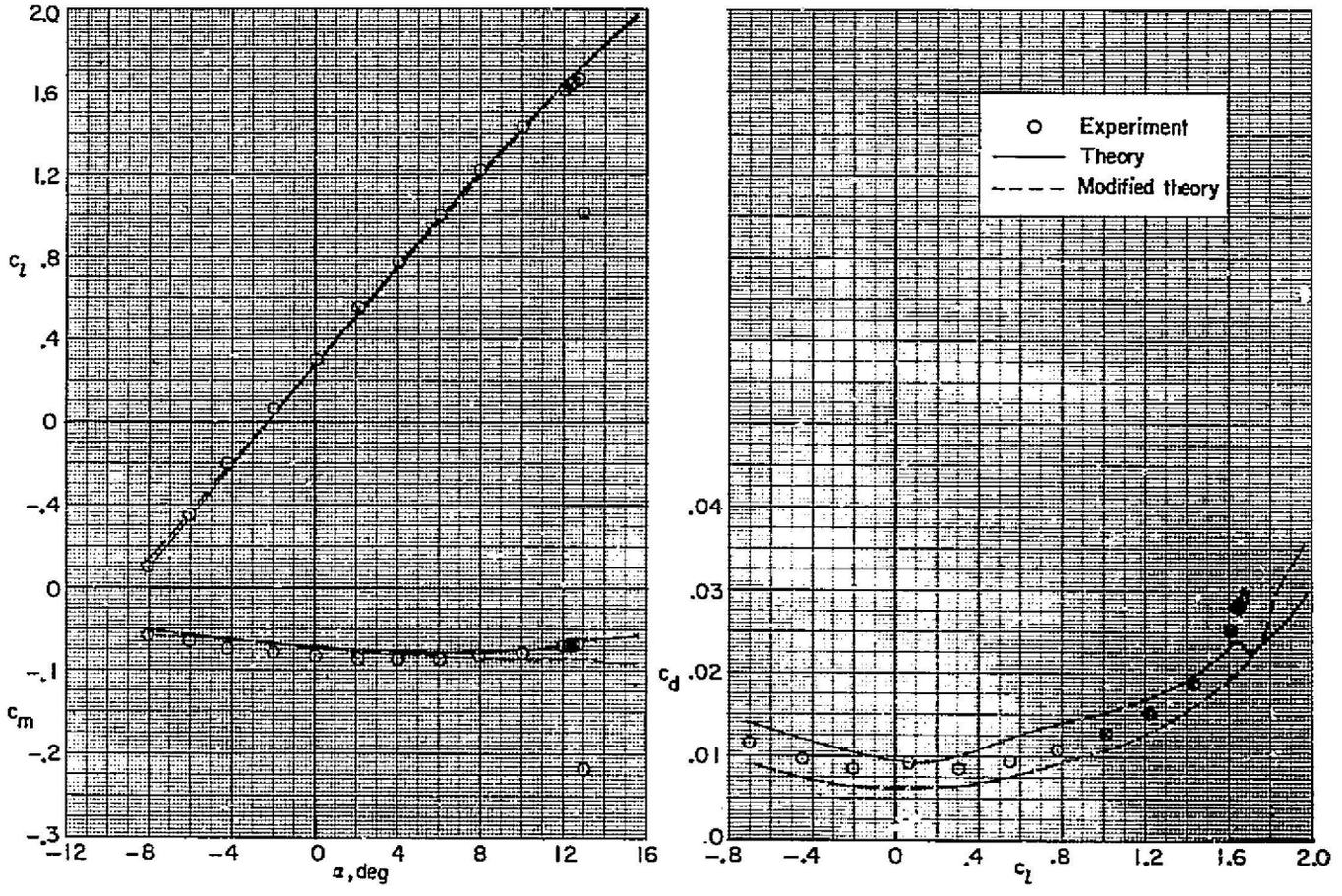


(a) $R = 2.9 \times 10^6$.

Figure 16.- Comparison of section coefficients with theory. $M = 0.20$.

(b) $R = 16.8 \times 10^6$.

Figure 16.- Concluded.